Regulation of DNA double-strand breaks during meiotic prophase in the nematode *C. elegans*

Heyun Guo

Regulation of DNA double-strand breaks during meiotic prophase

in the nematode C. elegans

By

Heyun Guo

A dissertation submitted in partial fulfillment of the

requirements for the degree of

Doctor of Philosophy

in

Life Sciences

in the Graduate School of Biostudies

of

Kyoto University

August 2022

Abstract

Proper chromosome segregation during meiosis depends on chiasmata, which are created by crossover recombination between homologous chromosomes. Meiotic recombination is initiated by programmed double strand breaks (DSBs) catalyzed by endonuclease Spo-11. Since either too many or too few DSBs could create problems for the germ cells, the level of DSBs must be under strict regulation. Here, I show that in *Caenorhabditis elegans*, meiotic DSB levels are tuned by the phosphoregulation of DSB-1 via the opposite roles played by PPH-4.1 phosphatase and ATL-1 kinase, in which PPH-4.1 counteracts the anti-DSB activity of ATL-1 and thus promotes DSB initiation to ensure sufficient crossover formation for the proper chromosome segregation. Moreover, reducing the phosphorylation of DSB-1 does not only increase the DSB levels but also rescue the homologous pairing and synapsis defects in *pph-4.1* mutants, which further reinforces the idea that homologous synapsis is strengthened by DSBs in *C. elegans.* In addition, I also show the phosphorylation level of DSB-1 increases with age and upon the loss of its paralog, DSB-2; while preventing DSB-1 phosphorylation rescues the reduced DSB activity in *dsb-2* mutants. These results suggest PPH-4.1 phosphatase, ATL-1 kinase and DSB-2 work together with DSB-1 to ensure optimal levels of DSBs for sexual reproduction.

I dedicate my work to my parents,

whose constant love and encouragement support me to reach here today,

and to my grandparents,

who were always proud of me for better or worse.

Table of Contents

List of Tables and Figures

Chapter 1:

Chapter 2:

Chapter 3:

Chapter 4:

Acknowledgement I

This thesis is based on material contained in the following scholarly paper.

Heyun Guo, Ericca L. Stamper, Aya Sato-Carlton, Masa A. Shimazoe, Xuan Li, Liangyu Zhang, Lewis Stevens, KC Jacky Tam, Abby F. Dernburg, Peter M. Carlton.
Phosphoregulation of DSB-1 mediates control of meiotic double-strand break activity.
eLife, volume 11, 2022. DOI: https://doi.org/10.7554/eLife.77956.

Acknowledgement II

I would like to first thank my supervisor, Dr. Peter Carlton, who has supported me so much in study and research throughout my doctoral career. He is an extremely kind and responsible advisor who is always around students and providing his help. I learned from him that in addition to being rigorous, staying tenacious is also critical for scientific research. His guidance will leave a profound influence both on my future career and my life. Thanks to Aya Sato-Carlton for teaching me all the experimental skills and providing invaluable discussions as well as technical help to my project. Thanks to the other current and former members in Carlton Lab: Carlos Rodriguez, Xuan Li, Andrea Ruelas, Keita Kameda, Makiko Nishimura, Masaaki Shimazoe, Takaya Hashimoto, Minami Murai, Jacky Tam, Tjebbe Boersma, Daria Doncevic and Yoshihisa Tanaka, for their support in both research and daily life. I would also like to thank Dr. Makoto Hayashi and all the members from his lab for expanding my horizons to other scientific fields and supporting my study in Japan.

I would like to express my gratitude to my parents, who are standing by me with their selfless love all the time no matter what happens. I thank my best friends: Xingxing Qi and Mengdi Zhou, who are always supporting me by patient listening and continuous encouragement throughout the ups and downs. I also want to thank Dr. Wanzhen Zhang and Dr. Yan Li for their kind understanding and emotional support.

Studying and working as a PhD candidate is quite a long journey, and now I am approaching the end of it. However, the most exciting part is not the destination but the process itself. All the mentors, classmates and friends I met; all the experience I gained from the failures and successes during this journey is a memorable and incredible treasure for me, which will be of benefit to my whole life.

Abbreviations

DSB: double strand break

CO: crossover

SC: synaptonemal complex

NHEJ: nonhomologous end joining

RMM: Rec114, Mei4 and Mer2 complex

PC: pairing center

NGM: nematode growth medium

RNAi: RNA interference

IP: immunoprecipitation

AID: auxin-inducible degradation

MSA: multiple sequence alignment

FISH: fluorescence in situ hybridization

WT: wild type

Chapter 1

Introduction

1.1 Overview of meiosis

Meiosis is a special type of cell division required for sexual reproduction. In this process, after a single round of DNA replication and two rounds of chromosome segregation, the number of chromosomes in one parent cell reduces by half to produce haploid gametes, such as sperm or egg cells. This reduction in ploidy is essential to guarantee the restoration of diploidy in the next generation upon fertilization (Hillers et al., 2017).

The two rounds of chromosome segregation are known as meiosis I and meiosis II respectively (**Figure 1.1**). In meiosis I, the homologous chromosomes pair with each other, synapse and exchange genetic information through recombination, which result in the formation of chiasma, a physical connection between the homologous chromosomes and enable the proper chromosome segregation during the first cell division (Hunter, 2015) (**Figure 1.1**). Since the number of chromosomes is reduced by half during this time, meiosis I is also referred to as a reductional division. In meiosis II, similar to mitosis, the sister chromatids segregate, creating haploid daughter cells. Two haploid gametes containing one copy of each chromosome fuse during fertilization and form a diploid cell with a complete set of paired chromosomes in the next generation (**Figure 1.1**).

It is crucial to understand the mechanism of meiosis since the misregulation of meiosis usually results in aneuploidy, which is a major cause of infertility and developmental disabilities (Hunt & Hassold, 2008).

1.2 Meiotic prophase I

Meiosis I is further divided into prophase I, metaphase I, anaphase I, and telophase I stages, among which prophase I is by far the longest phase of meiosis. Meiotic prophase I is further divided into several substages which are named based on the appearance of chromosomes: Leptotene, zygotene, pachytene, diplotene and diakinesis.

Many key events happening at these substages of prophase I are tightly coordinated in order to guarantee the accuracy of chromosome segregation. DNA replication occurs before meiosis begins, resulting in two identical sister chromatids held together through cohesion. Right after DNA replication, meiotic cells enter the leptotene stage, also known as leptonema, derived from Greek words meaning “thin threads”, in this stage, the chromosomes condense from diffuse chromatin into thin and long strands. Leptotene is followed by zygotene stage, also derived from Greek words meaning “paired threads”, and at

this time, each chromosome identifies its homologous partner and aligns with it, which is called homologous pairing. Meiotic recombination also initiates in this stage by the formation of DNA double strand breaks (DSBs) created by SPO-11 enzyme. Later, the paired homologous chromosomes become more closely linked and the pairing is forced to be more stable by the assembly of a protein structure called synaptonemal complex (SC) between the aligned chromosomes. All chromosomes are fully synapsed in pachytene stage; in the meantime, recombination is completed through the repair of double strand breaks. A subset of break repair results in the formation of crossovers (COs), which create physical links between each paired chromosome and forms a structure called chiasma which is visible upon chromosome structural remodeling in diplotene and diakinesis stages. In diakinesis, the chromosomes are more condensed and the homologous chromosomes also known as bivalents are still tightly bound at chiasmata; this helps to direct the homologs to segregate away from each other and proceed to the first meiotic cell division (Hillers et al., 2017).

1.3 Meiotic recombination and double strand formation

For most species, homologous recombination is vital for the proper chromosome segregation during meiosis (Davis & Smith, 2001). The crossovers formed through recombination act to tether homologous chromosomes together and make them attach correctly to the meiosis I spindle, which in turn, orient the homologs so they segregate away from each other and move to opposite poles during the first meiotic division (Hillers et al., 2017). The loss of meiotic recombination and thus the lack of crossovers usually lead to the missegregation of homologs and the resulting aneuploid gametes give rise to defective or inviable progeny (Davis & Smith, 2001). In addition, as a result of meiotic recombination, an individual chromatid can be composed of both maternal and paternal genetic information, resulting in a unique offspring that is genetically different from either parent. Moreover, a single gamete can contain a mix of maternal, paternal as well as recombinant chromatids. This genetic diversity generated by recombination is a benefit for the evolution of the species.

Meiotic recombination is initiated by the programmed introduction of DSBs which is created by the topoisomerase-like protein SPO-11 (Hinman et al., 2021a; Keeney, 2008). The single stranded DNA filaments generated from the DSB formation are coated by RAD-51 and DMC-1, which are involved in the homologous chromosome invasion (Bishop et al., 1992; Shinohara et al., 1992, 1997; Zickler & Kleckner, 2015). In the context of the assembled SC between the aligned homologs, recombination is then processed through the repair of these breaks using the homologous chromosome as a repair template. A majority of the DSBs are

repaired without forming crossovers, leading to gene conversion (Chen et al., 2007). However, a subset of break repair results in the formation of COs, which plays an essential role in proper chromosome segregation.

The DSB initiation must be strictly regulated, due to the potential harms they may bring: the remaining unrepaired DSBs may trigger the DNA damage response, leading to apoptosis and genetic instability (Bhalla & Dernburg, 2005; Roeder & Bailis, 2000). Additionally, error-prone DSB repair mechanisms such as nonhomologous end joining (NHEJ) may generate a high frequency of deletions or insertions in the genome as well as large-scale genome rearrangements (S. Kim et al., 2016; Lieber, 2008). In spite of these hazards, decificient DSBs may cause a failure in CO formation, and thus unattached homologs (univalents) that can't segregate evenly during the meiotic divisions, which in turn, leads to the production of aneuploidy in the next generation (Hinman et al., 2021b). Thereby, the level of DSBs must be governed tightly to achieve a number which is not too high, but not too low, in order to ensure enough DSBs are created to guarantee one CO per chromosome pair while limiting excess DSBs that may cause danger to the genome (Keeney et al., 2014). How these DSBs are regulated at a proper level for faithful meiosis is still a mystery.

In addition to the topoisomerase-like protein SPO-11, other factors also play critical roles in the regulation of DSB formation (Keeney, 2008; Keeney et al., 1997). Rec114, Mei4 and Mer2, together referred to as the RMM complex, were originally discovered through genetic screens in *Saccharomyces cerevisiae* designed to identify genes required for initiation of recombination (Malone et al., 1997; Menees & Roeder, 1989). Homologs of Rec114 involved in DSB formation have been identified in several species, including Rec114 in *Mus musculus* (Kumar et al., 2015, 2018) and Rec7 in *Schizosaccharomyces pombe* (Malone et al., 1997; Molnar et al., 2001). *Caenorhabditis elegans* DSB-1 and DSB-2 are also recognized as the distant orthologs of REC114 despite the high sequence divergence (Rosu et al., 2013; Stamper et al., 2013; Tessé et al., 2017). Furthermore, *Caenorhabditis elegans* DSB-3, which is also required for DSB formation, has been identified as a homolog of Mei4 and interacts with DSB-1 based on recent research (Hinman et al., 2021b).

1.4 Meiosis in Caenorhabditis elegans

Among the organisms studied for meiosis, *C. elegans* has emerged as an ideal model for meiotic mechanism investigation, which is not only because the worm germ line offers exceptional possibilities for high-resolution cytological analysis of chromosome and nuclear organization when using whole mount preparations that preserve 3D nuclear architecture

(Hillers et al., 2017; Phillips, McDonald, et al., 2009)), but germ cells in a germ line are organized in a spatial and temporal manner so that all stages of meiosis are displayed conveniently within the gonad of an individual animal (Phillips, McDonald, et al., 2009) (**Figure 1.2**).

Homologous pairing in *C. elegans* occurs during early meiotic prophase (leptotene and zygotene), which is also referred to as the transition zone. The region called paring center (PC) that is localized near one end of each chromosome plays an important role in chromosome movements and thus the initiation of pairing (McKim et al., 1988; Phillips, Meng, et al., 2009; Rose et al., 1984; Rosenbluth & Baillie, 1981; Villeneuve, 1994). Each PC is bound by one of four C2H2 zinc finger proteins: HIM-8 on the *X* chromosome, ZIM-1 on chromosomes *II* and *III*, ZIM-2 on chromosome *V*, and ZIM-3 on chromosomes *I* and *IV*. These proteins are both required for homologous pairing and synapsis (Phillips et al., 2005; Phillips, Meng, et al., 2009; Phillips & Dernburg, 2006).

Similar to other eukaryotes, meiotic DSBs in *C. elegans* are induced by SPO-11, but other factors are also essential for DSB formation. DSB-1 and DSB-2 are specifically required for DSB initiation (Rosu et al., 2013; Stamper et al., 2013). Moreover, MRE-11 (Chin & Villeneuve, 2001), RAD-50 (Hayashi et al., 2007), HTP-3 (Goodyer et al., 2008) as well as CHK-2 (MacQueen & Villeneuve, 2001) were also shown to be involved in the efficient production of meiotic DSB.

In other organisms such as budding yeast and mammals, synapsis is dependent on meiotic recombination since mutations in which DSB initiation or processing is abolished are also defective in synapsis (Baudat et al., 2000; Kleckner, 1996; Roeder, 1995; Romanienko & Camerini-Otero, 2000). However, in *C. elegans* and *Drosophila melanogaster*, homologous pairing and synapsis is capable of happening in the absence of recombination (Dernburg et al., 1998; McKim et al., 1998). Whereas *Caenorhabditis elegans* may achieve “normal” synapsis even in the absence of DSB formation, recent research has shown that such SCs formed in fact differ from normal SCs. The recombination-independent form of the *C. elegans* SC in early-phase is more dynamic/unstable, which may function to mediate/maintain homolog juxtaposition to enable engagement of the homologous chromosome by processed DSBs, while the late-phase form of SC between homologs is stabilized by recombination (Machovina et al., 2016; Pattabiraman et al., 2017; Roelens et al., 2015). But it is still unknown whether recombination normally contributes to homologous pairing and synapsis in *C. elegans*.

1.5 ATM-1^{ATM}/ATL-1^{ATR}-dependent phosphorylation of DSB-1

To prevent further DNA damage as well as allow for repair prior to the meiotic divisions, DSB formation must be shut down during meiotic prophase. In mammals (Lange et al., 2011), Drosophila (Joyce et al., 2011) and budding yeast (Carballo et al., 2013; Garcia et al., 2015; Zhang et al., 2011), DSBs have been reported to be down-regulated by the ATM/ATR family of DNA damage response kinases. The phosphorylation of Rec114, one of the SPO-11 accessory proteins, through budding yeast ATM/ATR (Tel1/Mec1) reduces both DSB formation and the interaction of Rec114 with chromosome regions highly likely to be cut by SPO-11, known as DSB-hotspots (Carballo et al., 2013; Garcia et al., 2015; Mohibullah & Keeney, 2017). Moreover, activation of ATR(Mec1) by replication stress can reduce the loading of REC114 on chromosomes in budding yeast (Blitzblau & Hochwagen, 2013). In addition, ATM and ATR kinases in mice both function to remove the recombination factors which are nearby the DNA breaks and suppress DSB initiation (Dereli et al., 2021; Lange et al., 2011).

In *C. elegans,* DSB-1 has been identified as an essential factor specifically required for DSB formation (Stamper et al., 2013) as well as a distant ortholog of REC114 (Tessé et al., 2017). More importantly, it has been shown that DSB-1 is phosphorylated in response to DSBs, in a manner dependent on ATM (ATM-1) and ATR (ATL-1) kinases (Stamper, 2014). This phosphorylation has been hypothesized to down-regulate meiotic DSB formation in order to limit the number of DSBs and prevent excess DSB levels accumulation (Stamper, 2014), which is similar to what has been found in other organisms. However, it is still unclear if any phosphatase acts to inhibit or regulate the anti-DSB activity of ATM and ATR kinases.

1.6 The function of PPH-4.1^{PP4} phosphatase in *C. elegans* meiosis

ATM and ATR phosphorylated substrates are known to be dephosphorylated in a wide range of contexts by the highly-conserved serine/threonine protein phosphatase 4 (PP4) (Hustedt et al., 2015; Keogh et al., 2006; J.-A. Kim et al., 2011; Lee et al., 2010). In budding yeast, PP4 has been demonstrated to regulate the non-homologous clustering of centromeres during early meiotic prophase by dephosphorylating Zip1, a central element of SC. Furthermore, PP4 plays an independent role in budding yeast SC formation (Falk et al., 2010).

In *C. elegans*, protein phosphatase PP4 (PPH4.1) has been characterized as playing multiple and separate roles during meiotic prophase (Sato-Carlton et al., 2014). PPH-4.1 activity is essential for four steps of meiotic prophase: First, it is required for synapsis-

independent pairing of autosomes while the pairing on chromosome *X* is fine without PPH-4.1. Second, PPH-4.1 functions in restricting the synapsis to homologous chromosomes and thus preventing synapsis between non-homologous partners or self-synapsis. Third, PPH-4.1 is necessary to achieve programmed DSB initiation. Last, PPH-4.1 is needed for CO formation (Sato-Carlton et al., 2014). Despite the several crucial and independent roles of PPH-4.1 in meiosis, the mechanism study on the meiotic functions of PPH-4.1, such as how it promotes the normal level of DSB production, still needs to be elucidated.

The requirement of PPH-4.1 in multiple meiotic stages is likely to result from the proper phosphoregulation of one or more proteins required for meiotic prophase. To identify these substrates of PPH-4.1 and to shed light on how the phosphorylation and dephosphorylation of these substrates are balanced to regulate the chromosome dynamics during meiosis are very promising perspectives in the field of meiosis study.

1.7 Overview of current work

My current work shows that the homeostasis of meiotic DSB levels is controlled by the phosphoregulation of protein DSB-1. During meiotic prophase, ATL-1-dependent DSB-1 phosphorylation inhibits DSB formation, which protects the genome against excessive DSBs which may endanger genome integrity. On the other hand, DSB-1 is dephosphorylated in a manner dependent on PPH-4.1 in order to ensure that at least one crossover occurs on each chromosome pair and guarantee the proper segregation of all chromosomes. Due to the fact that ATM/ATR kinases are activated by DNA breaks, this model implies that the activated ATR kinase shuts down the DSB machinery through DSB-1 phosphorylation once adequate levels of recombination intermediates have been generated. This feedback mechanism could safeguard the DSBs at an appropriate level for the accurate meiotic progression via DSB-1 phosphorylation.

In Chapter 2, I will discuss the identification of a DSB-promoting pathway regulated through the dephosphorylation of protein DSB-1 by PPH-4.1^{PP4} phosphatase. DSB-1 is dephosphorylated in a PPH-4.1^{PP4}-dependent manner and blocking the phosphorylation on the five serines within the five SQ motifs of DSB-1 can increase the DSB levels and rescue the DSB formation defect in *pph-4.1* background. Furthermore, I also find that the homologous pairing and synapsis defects in *pph-4.1* mutants are rescued upon the elevated DSB levels when DSB-1 is not phosphorylatable, which strongly suggests that DSBs can strengthen homologous synapsis in *C. elegans.*

In Chapter 3, I will describe the function of DSB-1 phosphorylation with or without DSB-2, a paralog of DSB-1, which is required for normal levels of DSB formation. The DSBs formed in the presence of the DSB-1 non-phosphorylatable allele are fully insensitive to the absence of DSB-2. Both the reduced protein amount and increased phosphorylation level of DSB-1 contribute to the few numbers of DSBs upon the loss of DSB-2 in young animals. Moreover, when DSB-2 is present, the phosphorylation of DSB-1 appears to be increased with age, which is responsible for the reduction of DSB initiation in older animals in wild type condition. I also find S186 among the five serines of DSB-1 plays a determinant role in DSB formation when DSB-2 is absent. Additionally, I predict a model in which DSB-1 forms a heterotrimeric complex with DSB-2 and DSB-3, and it is more likely that DSB-1 dimers are bound to DSB-3 in the absence of DSB-2, rather than DSB-2 dimers bind to DSB-3 when DSB-1 is absent, which helps to explain the worsen DSB formation defect in *dsb-1* mutants than *dsb-2* mutants.

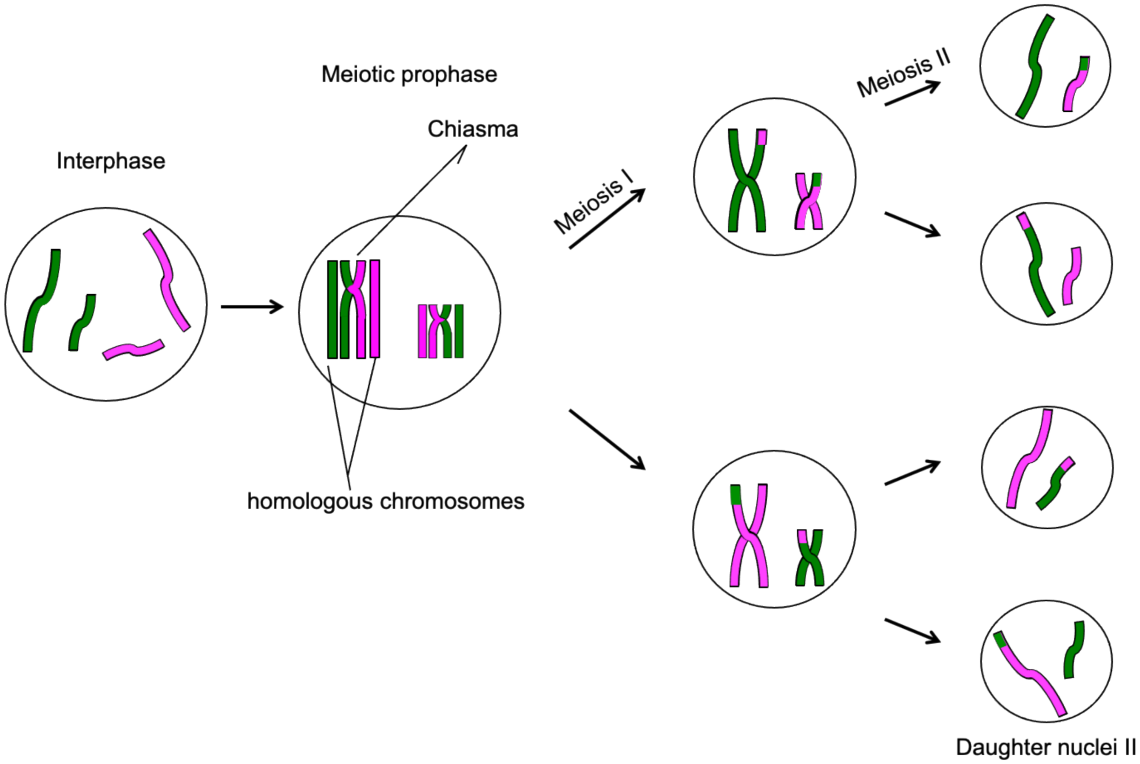

Figure 1.1 Diagram showing the meiotic progression. During Meiosis I, genetic information is exchanged through recombination between homologous chromosomes and followed by the segregation of each pair of homologous chromosomes. In Meiosis II, sister chromatids split up to form haploid gametes.

A

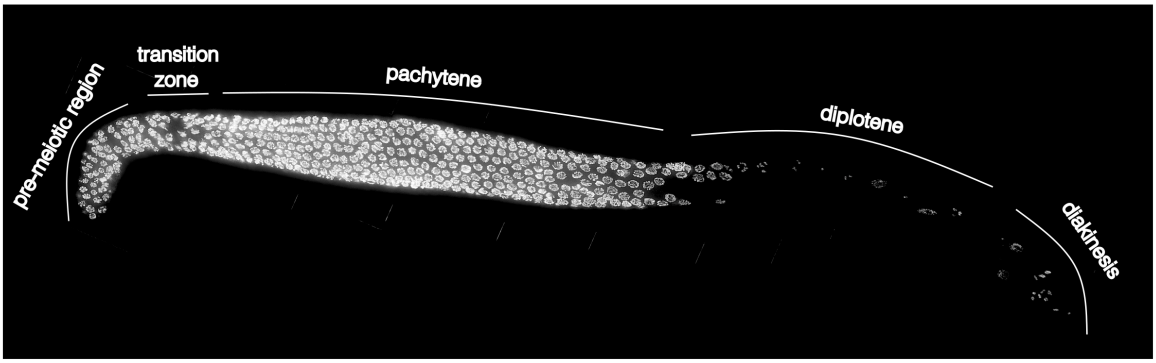

B

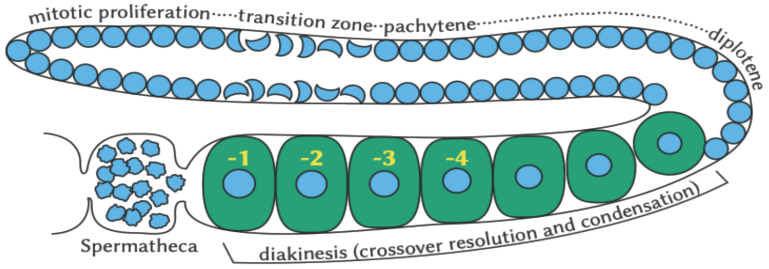

Figure 1.2 Meiotic progression in *C. elegans*. (A) Entire gonad of a wild type animal stained with DAPI. The meiotic prophase stages are shown clearly throughout the germline. **(B)** Diagram depicting the meiotic prophase in *C.elegans*.

Chapter 2

Identification of a DSB-promoting pathway regulated by DSB-1 dephosphorylation through PPH-4.1^{PP4} phosphatase

2.1 Introduction

To generate haploid gametes from diploid gametes during meiosis, the number of chromosomes must be reduced by half through chromosome segregation. Accurate chromosome segregation during the first meiotic cell division relies on chiasmata to tether the homologous chromosomes together in the first place, which is an outcome of meiotic recombination. The recombination is initiated by the programmed DSBs created by the topoisomerase-like protein SPO-11 (Hinman et al., 2021a; Keeney, 2008). Either too high or too low levels of DSBs is dangerous to the genome: the excess DNA damage resulting from unpaired DSBs often leads to apoptosis, while insufficient DSBs cannot achieve at least one crossover per chromosome after DNA repair so that the chromosomes cannot segregate properly, which in turn, results in the formation of aneuploidy and embryonic lethality. Thus, the DSB formation needs to be tightly controlled at an appropriate level to ensure the complete meiotic progression.

In *C. elegans*, protein DSB-1 has been identified to be phosphorylated depending on DNA damage response kinases ATM and ATR, and the phosphorylation acts to limit the number of DSBs which appears to prevent the genome from toxic DNA damage (Stamper, 2014). But no phosphatase has been found to antagonize ATM/ATR kinases in this pathway. Here I describe that DSB-1 is dephosphorylated in a protein phosphatase PPH-4.1-dependent manner, which counteracts the anti-DSB activity of ATR kinase and promotes DSB formation so that the number of DSBs can be achieved to a proper level for the successful crossover formation during meiosis. Moreover, blocking the phosphorylation of DSB-1 does not only restore the DSBs reduced by the loss of PPH-4.1, but also partially rescue non-homologous pairing and synapsis defects in the absence of PPH-4.1, which highly suggests that DSB formation also contributes to the fidelity of pairing and synapsis in *C. elegans*.

2.2 Materials and methods

2.2.1 *C. elegans* strains and culture conditions

Worm strains were maintained at 20 °C on nematode growth medium (NGM) plates seeded with OP50 bacteria under standard conditions (Brenner, 1974). Bristol N2 was used as the wild type strain and all mutants were derived from an N2 background. Strains used in this study are shown as below:

- PMC575 *icm97 [gfp-dsb-1](IV)*
- PMC569 *icm98 [dsb-1(S137A_S143A_S186A_S248A_S255A)](IV)*
- OC271 *pph-4.1(tm1598)/hT2[bli-4(e937) let-?(q782) qIs48](I;III)*

- PMC583 *pph-4.1(tm1598)/hT2[bli-4(e937) let-?(q782) qIs48](I;III); icm97 [gfp-dsb-1](IV)*
- PMC594 *pph-4.1(tm1598)/hT2[bli-4(e937) let-?(q782) qIs48](I;III); icm98 [dsb-1(S137A_S143A_S186A_S248A_S255A)](IV)*
- DW101 *atl-1(tm853) V/nT1[unc-?(n754) let-? qIs50] (IV;V)*
- PMC253 *pph-4.1(tm1598)/hT2[bli-4(e937) let-?(q782) qIs48](I;III); atl-1(tm853)/nT1[let-? unc-?(n754)](IV;V)*
- PMC188 *atm-1(gk186)/hT2; pph-4(tm1598)/hT2[bli-4(e937) let-?(q782) qIs48](I;III)*
- PMC193 *atm-1(gk186) rad-54(ok615)/hT2[bli-4(e937) let-?(q782) qIs48](I;III)*
- VC531 *rad-54&snx-3(ok615) I/hT2[bli-4(e937) let-?(q782) qIs48] (I;III)*

2.2.2 Generation of mutants via CRISPR-Cas9 genome editing system

CRISPR-Cas9 genome editing using *dpy-10* as co-CRISPR marker (Arribere et al., 2014) was applied to generate *gfp-dsb-1* and dsb-1 non-phosphorylatable mutant *dsb-1(5A)*. A 10 µL mixture containing 17.5 µM trans-activating CRISPR RNA (tracrRNA)/crRNA oligonucleotides (targeting *dsb-1* and *dpy-10*) purchased from Integrated DNA Technologies (IDT), 17.5 µM Cas9 protein produced by the MacroLab at UC Berkeley, and 6 µM single-stranded DNA oligonucleotide purchased from IDT (for *dsb-1(5A)*) or 150 ng/µL double-stranded DNA generated from PCR (for *gfp-dsb-1*) as a repair template was injected into the gonads of 24 h post-L4 larval stage N2 hermaphrodites. To prevent re-editing by the CRISPR-Cas9 machinery, silent mutations were introduced into the target gene dsb-1. For *gfp-dsb-1*, an additional linker sequence of 3x glycine was introduced between the target site and GFP-tag sequence. Dpy or Rol F1 animals (dpy-10 mutation homozygous or heterozygous, respectively) were picked to individual plates to self-propagate overnight and then screened for successful edits by PCR and DNA sequencing. A list of oligonucleotides used is provided as below:

- Alt-R® CRISPR-Cas9 tracrRNA (Cat# 1072532, IDT)
- dpy-10 crRNA: 5'-GCTACCATAGGCACCACGAG-3'
- *gfp-dsb-1* CRISPR crRNA1: 5'-CTGAATTGCAGACACTCCAG-3'
- *gfp-dsb-1* CRISPR crRNA2: *5'*-AATTGCTTATACTTTATGAT-3'
- *dsb-1(S137A_S143A_S186A_S248A_S255A)* CRISPR crRNA1: 5'-AGGTGCGTTTGCGGGACTGG-3'
- *dsb-1(S137A_S143A_S186A_S248A_S255A)* CRISPR crRNA2: 5'-GAAAATGACGAACTGTGCGA-3'
- dpy-10(cn64) homology template for CRISPR: 5'-cacttgaacttcaatacggcaagatgagaatgactggaaaccgtaccgcATgCggtgcctatggtagcggagcttcacatggcttcagaccaacagcct-3'

- *gfp-dsb-1* homology template for CRISPR: 5'-
caataattttatctgcgatcccaatatgtacagctacgatcccttctcacatacttcctgtgcctgtattttatttatttttattttttctttcttcaacgaaccattactatacgggttcccgcttccgaataccgccttttgactattattccctgcattttcgtgtgaatcattgctcccaagtactcattttgccttccatttggctttaatttattgcagtttgtcgtcataataaacttttttatcaatttatcaaaaatttttattttatctattacataaatgcgattaaatttttaagttaaaaaaacgagaattagctaaattagatatgcttggtaatttgaatttgaattcgcgcgtaaaagtgatggatgggtctcgccacgaccggcatgcaattttgaatttttttcacattttgaggtccaatgaCgtcgaaatttttagacatttttagtaaaaaaaaattatttatgtttttgcagtctcttcagtATGAGTAAAGGAGAAGAATTGTTCACTGGAGTTGTCCCAATCCTCGTCGAGCTCGACGGAGACGTCAACGGACACAAGTTCTCCGTCTCCGGAGAGGGAGAGGGAGACGCCACCTACGGAAAGCTCACCCTCAAGTTCATCTGCACCACCGGAAAGCTCCCAGTCCCATGGCCAACCCTCGTCACCACCTTCTGCTACGGAGTCCAATGCTTCTCCCGTTACCCAGACCACATGAAGCGTCACGACTTCTTCAAGTCCGCCATGCCAGAGGGATACGTCCAAGAGCGTACCATCTTCTTCAAGgtaagtttaaacatatatatactaactactgattatttaaattttcagGACGACGGAAACTACAAGACCCGTGCCGAGGTCAAGTTCGAGGGAGACACCCTCGTCAACCGTATCGAGCTCAAGgtaagtttaaacagttcggtactaactaaccatacatatttaaattttcagGGAATCGACTTCAAGGAGGACGGAAACATCCTCGGACACAAGCTCGAGTACAACTACAACTCCCACAACGTCTACATCATGGCCGACAAGCAAAAGAACGGAATCAAGGTCAACTTCAAGgtaagtttaaacatgattttactaactaactaatctgatttaaattttcagATCCGTCACAACATCGAGGACGGATCCGTCCAACTCGCCGACCACTACCAACAAAACACCCCAATCGGAGACGGACCAGTCCTCCTCCCAGACAACCACTACCTCTCCACCCAATCCGCCCTCTCCAAGGACCCAAACGAGAAGCGTGACCACATGGTCCTCCTCGAGTTCGTCACCGCCGCCGGAATCACCCACGGAATGGACGAGCTCTACAAGggaggtggaATGTTTCCaGAgcTcCAaACcCTtCAaTGGCCGATtATcAAGTAcAAGCAgcTcAGAGGAAGCGGTAATCGACAAGAGgttttaaaaatagatgaattctgtatcgaaaagttaaatttgcagGGCAAAGATATTCGCGTTGTTATGGAGGTGAATAGCAGGAAGCTGACGGTTATTCATGGAGTCGAGCCGATCGAGACCGTTTATTGTAACATGGAAGTTTCTAGGTATCCGAGTTTGAAgtgagtctttgttgtttgagaaattaaagtcaaattgcccggttttcagAATGAAGAACACAAATTTGTTCGTGATTGTAAACAACCAGGCTCAAGGTTTCCGATTAACTCTTCGTGGCGAAGATCGGGAGAATTTTCTGTCAACTGTCAGAAAATTTGCTTATATTTCGGAGACTCCAGTTAAGGATCATTTGAATCGCTCATCCACAAATACCGgtattctttattcttttaatagtttcaagtttc-3'
- *dsb-1(S137A_S143A_S186A_S248A_S255A)* homology template for CRISPR: 5'-
GCCAAATTCGAACCATTCTTTGCAATTTCCGTGTCCCAGCCCATCtCAttccTCtTCtTTcTCtGGtTTcgCtCAGgtaaattgaaaattaactggaatatcccaccctattaaattaattttcagAGTTCATCACACTCTgCcCAATTGTCtTCCAGTCCCGCAAACGCACCTTCATTTCCGGATTTTCACAGCCCACC-3'
- *gfp-dsb-1* genotyping forward primer: 5'-TGCGATCCCAATATGTACAGCT-3'

- *gfp-dsb-1* genotyping reverse primer: 5'-TACCGGTATTTGTGGATGAGCG-3'
- *dsb-1(S137A_S143A_S186A_S248A_S255A)* genotyping forward primer: 5'-TCCTCTTCTTTCTCTGGTTTCGC-3'
- *dsb-1(S137A_S143A_S186A_S248A_S255A)* genotyping reverse primer: 5'-GAACGCATTTGTCCGCAGTT-3'

2.2.3 RNA interference

RNAi was carried out by feeding N2 or gfp-dsb-1 worms with the HT115 bacteria expressing either the empty RNAi vector L4440 obtained from the Ahringer Lab RNAi library (Kamath et al., 2003) or a pph-4.1 RNAi plasmid (Sato-Carlton et al., 2014). Worms were first synchronized through starvation and grown to the L4 larval stage on new NGM plates with OP50 bacteria. L4 worms were collected in M9 (41 mM Na2HPO4, 15 mM KH2PO4, 8.6 mM NaCl, 19 mM NH4Cl) + 0.01% Tween buffer, washed three times with M9 buffer and distributed to RNAi plates. About 30 h later, the worms became gravid and were harvested in M9 + 0.01% Tween buffer, washed three times with M9 buffer and bleached for no more than 3 min to obtain F1 embryos. Collected embryos were placed to fresh RNAi plates and grown until 24 h after the L4 larval stage. For the immunoprecipitation experiment, worms were harvested in M9 + 0.01% Tween buffer and exposed to 10Gy γ-irradiation, and then washed two times with M9 buffer. Lastly, the worms were washed with RIPA buffer (150 mM NaCl, 1% Triton X-100, 0.5% Sodium deoxycholate, 0.1% SDS, 50 mM TrisHCl pH 8.0) + 1mM PMSF +1mM DTT and the supernatant was poured off until 2x pellet volume. Worm pellet suspensions were then supplemented with 2x protease inhibitor cocktail + 3mM NaF, frozen in liquid nitrogen and stored at -80 °C. For western blot analysis, worms were harvested and washed three times in M9 buffer and frozen in liquid nitrogen.

2.2.4 Immunoprecipitation and phosphatase assay

Immunoprecipitation of GFP-tagged DSB-1 was performed with the same amount of lysate determined by BCA kit (Pierce BCA protein assay kit #23225, Thermo Scientific) from wild type and pph-4.1 RNAi animals. Protein samples were incubated with GFP-Trap (ChromoTek #gtma-20) at 4 °C overnight with gentle rotation and the collected beads were washed three times with wash buffer (10 mM Tris/Cl pH 7.5, 150 mM NaCl, 0.05 % Nonidet P-40, 0.5 mM EDTA). The beads to which GFP-DSB-1 had been immobilized were subject to the phosphatase assay (NEB lambda phosphatase #P0753S) following manufacturer's instructions at 30 °C for 2 h. Then the protein was eluted in the SDS-PAGE sample buffer by boiling at 95 °C for 10 min and used for western blotting.

2.2.5 Auxin-induced protein depletion in worms

Depletion of AID-tagged proteins in the *C. elegans* germline was performed as previously described (Zhang et al., 2015). Briefly, 1mM auxin (IAA, Alfa Aesar #10556) was added into the NGM agar just before pouring plates. E. coli OP50 bacteria cultured overnight were concentrated, supplemented with 1mM auxin and spread on plates. These auxin plates were stored at 4 °C in the dark and used within a month. NGM plates supplemented with the solvent ethanol (0.25% v/v) were used as control. To obtain synchronized worms, L4 hermaphrodites were picked from the maintenance plates. Auxin treatment was performed by transferring worms to auxin plates and incubating for the indicated time at 20 °C. Young adult animals (24 h post-L4) were dissected for immunofluorescence analyses.

2.2.6 Lysate preparations

For immunoprecipitation, frozen RNAi worms were milled using the Mixer Mill MM 400 (Retsch; cycle at 25 times/sec for 2 min, 3 cycles total). Worm powder was thawed on ice and sonicated using an ultrasonic disruptor (UD201; Tomy Tech.) with gauge at number 10, 5 times (20 sec followed by 1 min rest each time). To the lysate, 5 mM MgCl2 and 125 U/ml Benzonase were added, and the lysis was continued by rotating at 4 °C for 30 min. The lysate was then spun down at 22000 g for 20 min at 4 °C, and the supernatant was filtered with 40 μm cell strainer (Corning Falcon #352340) and saved at -80 °C.

To prepare samples for general western blotting of GFP-fused DSB-1 from animals treated with or without *pph-4* RNAi, frozen worm pellet was suspended in urea lysis buffer (20 mM HEPES pH 8.0, 9M Urea, 1 mM sodium orthovanadate), sonicated (Taitec VP505 homogenizer; 50% output power, cycle of 10 sec on and 10 sec off for 7 min total) and spun down at 16000 g at 4 °C for 15 min. The supernatant was used to measure protein concentration using the BCA kit (Pierce BCA protein assay kit #23225; Thermo Scientific), and a total protein amount of 97 μg was loaded for western blotting after boiling for 10 min in SDS-PAGE sample buffer.

2.2.7 Western blotting

For western blotting of GFP-fused DSB-1, SDS-PAGE was carried out using 5-12% Wako gradient gel (Wako #199-15191), and proteins were transferred to a PVDF membrane at 4 °C, 80 V for 2.5 h. The membrane was blocked with TBST buffer (TBS and 0.1% Tween) containing 5% skim milk (Nacalai Inc. #31149-75) at room temperature for 1 h and probed with primary antibody solution containing 2.5% skim milk at 4 °C overnight followed by additional 2 h at room temperature, washed with TBST for four times, probed with secondary

antibody solution containing 2.5% skim milk at room temperature for 2 h, washed with TBST for four times. Chemi Luminol assay kit, Chemilumi-one super (Nacalai Inc. #02230-30) or Chemilumi-one ultra (Nacalai Inc. #11644-24), was used to visualize protein bands using an ImageQuant LAS4000 imager (GE Healthcare #28955810).

Antibodies and dilutions used in this study are shown as below:

- mouse anti-GFP (1:1000; Cat#sc-9996, Santa Cruz)
- rabbit anti-Actin (1:3000; Cat#sc-1615, Santa Cruz)
- guinea pig anti-DSB-1 (1:75; (Stamper et al., 2013))
- HRP-conjugated sheep anti-mouse (1:10000; Cat#NIF825, GE Healthcare Bio-Sciences)
- HRP-conjugated goat anti-rabbit (1:10000; Cat#ab97051, Abcam)
- HRP-conjugated goat anti-guinea pig (1:10000; Cat#732868, Beckman Coulter)

2.2.8 Immunofluorescence and imaging

Immunostaining was performed as described in (Phillips, McDonald, et al., 2009) with modifications as follows: Young adult worms (24 h post-L4 larval stage) were dissected in 15 µL EBT (27.5 mM HEPES pH 7.4, 129.8 mM NaCl, 52.8 mM KCl, 2.2 mM EDTA, 0.55 mM EGTA, 1% Tween, 0.15% Tricane) buffer, fixed by adding another 15 µL fixative solution (25 mM HEPES pH 7.4, 118 mM NaCl, 48 mM KCl, 2 mM EDTA, 0.5 mM EGTA, 1% Formaldehyde) and mixing for no more than 2 min in total on each coverslip. The excess liquid was pipetted off with 15 µL remaining which was picked up by touching a micro slide glass (Matsunami #S9901) to the top of it before freezing at -80 °C. The slides were fixed in -20 °C methanol for exactly 1 min, transferred to PBST (PBS and 0.1% Tween) immediately and washed 3 times (10 min/time) by moving slides to fresh PBST at room temperature. Then the slides were blocked in 0.5% BSA in PBST for 30 min. Primary antibody incubation was performed at 4 °C overnight while secondary antibody incubation was performed for 2 h at room temperature. At last each slide was mounted with 15 µL mounting medium (250 mM TRIS, 1.8% NPG-glycerol) onto clean Matsunami No. 1 1⁄2 (22 mm^2) coverslip.

Images were captured by a Deltavision personalDV microscope (Applied Precision/GE Healthcare) equipped with a CoolSNAP ES2 camera (photometrics) at a room temperature of 20-22 °C, using a 100x UPlanSApo 1.4NA oil immersion objective (Olympus) and immersion oil (LaserLiquid) at a refractive index of 1.513. The Z spacing was 0.2 µm and raw images were subjected to constrained iterative deconvolution followed by chromatic correction. Image acquisition and deconvolution was performed with the softWoRx suite

(Applied Precision/GE Healthcare). Image postprocessing for publication was limited to linear intensity scaling and maximum-intensity projection using OMERO (Burel et al., 2015).

Antibodies and dilutions used in this study are shown as below:

- rabbit anti-RAD-51 (1:10000; Cat#29480002, lot# G3048-009A02, SDIX/Novus Biologicals)
- rabbit anti-ZIM-3 (1:2000; (Phillips & Dernburg, 2006))
- guinea pig anti-SYP-1 (1:100; (Sato-Carlton et al., 2020))
- donkey-Alexa488-anti-rabbit (1:500; Cat#711-545-152, lot#109880, Jackson ImmunoResearch)
- donkey-DyLight649-anti-guinea pig (1:500; Cat#706-495-148, lot#95544, Jackson ImmunoResearch)

2.2.9 Fluorescence in situ hybridization and quantification

The pairing on the right arm of chromosome V was monitored with fluorescence in situ hybridization (FISH) probes that label the 5S rDNA locus as described in (Phillips, McDonald, et al., 2009) with modifications as follows: young adult worms (24 h post-L4 larval stage) were dissected in 15 µL EBT buffer and fixed by adding another 15 µL 1% paraformaldehyde for 1-2 min. The excess liquid was removed before freezing. The slides were fixed in -20 °C methanol for exactly 1 min, transferred to 2x SSCT (150 mM NaCl, 15 mM Na citrate pH 7, 0.1% Tween) immediately and washed 3 times (10 min/time) by moving slides to fresh 2x SSCT at room temperature. Next, the slides were put in a Coplin jar filled with EBFa (25 mM HEPES pH 7.4, 118 mM NaCl, 48 mM KCl, 2 mM EDTA, 0.5 mM EGTA, 3.7% formaldehyde) for another 5 min. After that, the slides were transferred to 2x SSCT and washed for 3 times (5 min/time) to remove the fixative. The slides were put into 50% formamide in 2x SSCT, incubated 10 min at 37 °C, and then transferred to a new jar with the same solution, incubated at 37 °C overnight. The probe solution (15 µL, (Dernburg et al., 1998)) was added onto a 22 x 22 mm coverslip. The worms on the slides were touched to the drop of probe solution on the coverslip until the liquid was spreaded out. After being sealed, the slides were denatured at 95 °C for 2 min 10 sec and incubated at 37 °C overnight. The slides were then washed with 50% formamide in 2x SSCT at 37 °C twice for a total of 1h, and washed with 2x SSCT for 10 min, stained with DAPI, washed again with 2x SSCT, and mounted with 15 µL mounting medium onto clean Matsunami No. 1S (22 mm^2) coverslip. Quantification of FISH foci was done as in (Sato-Carlton et al., 2014). FISH probes were generated as previously described (Dernburg et al., 1998).

2.2.10 RAD-51 foci quantification

Quantitative analysis of RAD-51 foci per nucleus was performed as in (Sato-Carlton et al., 2014). For all the genotypes except for rad-54 and atm-1; rad-54 mutants, manual counting was performed. For rad-54 mutants, semi-automated counting was used as below: for early zones (1 and 2) with very few RAD-51 foci, manual counting was performed. For zones 3 and above, programs (at github.com/pmcarlton/deltavisionquant) written in GNU Octave (Eaton et al., n.d.) were used to segment nuclei and count the number of RAD-51 foci in each nucleus. The nuclei on the coverslip-proximal side of the gonads were scored for each genotype. Statistical comparisons were performed via two-tailed t test.

2.2.11 DAPI body counting at diakinesis

For DAPI body counting, completely resolvable contiguous DAPI positive bodies were counted in three-dimensional stacks as described previously (Sato-Carlton et al., 2014). With this criterion, chromosomes that happen to be touching can occasionally be counted as a single DAPI body.

2.2.12 γ-irradiation assay

For DAPI body staining, late L4 larval stage worms were exposed to γ-rays for 58 minutes 30 seconds at 0.855 Gy/min (total exposure 50 Gy) in a Cs-137 Gammacell 40 Exactor (MDS Nordion). Irradiated worms were fixed 18-22 h after irradiation for DAPI staining and imaged to score DAPI-stained bodies as above. For immunoprecipitation of GFP-fused DSB-1, 24 h post-L4 worms were exposed to γ-rays for 11 minutes 42 seconds (total exposure 10 Gy).

2.2.13 Embryonic viability scoring

To score embryonic viability and male progeny of each genotype, L4 larval stage hermaphrodites (P0s) were picked individually onto plates and transferred to fresh plates every 24 h for 5 days. Unhatched eggs remaining on the plates 20 h after being laid were counted as dead eggs every day. Viable F1 progeny and males were scored 4 days after P0s were removed from corresponding plates.

2.2.14 Multiple sequence alignment

Protein sequences in the DSB-1/2 orthology group were retrieved from the Caenorhabditis Genomes Project (caenorhabditis.org). The protein prediction of DSB-1 for *C. latens* was found to be incomplete, so it was reconstructed by hand from the transcripts in Bioproject

PRJNA248912, from WormBase ParaSite version 14 (Howe et al., 2017). The sequences were then aligned using the L-INS-i setting of mafft v7.487 (Katoh & Standley, 2013).

2.3 Results

2.3.1 DSB-1 phosphorylation is prevented by PPH-4.1^{PP4} phosphatase

To test whether PPH-4.1 promotes DSB formation by regulating DSB-1, DSB-1 phosphorylation in the absence of PPH-4.1 was examined by western blotting. Worms carrying a GFP fusion of DSB-1 at the endogenous locus were treated either with RNAi against *pph-4.1* or an empty RNAi vector. The mutants of *gfp-dsb*-1 are as viable as wild type animals indicating the function of DSB-1 is not disrupted by the GFP fusion (**Figure 2.1A**). The effectiveness of *pph-4.1* RNAi was verified by the univalents stained by DAPI on diakinesis oocytes (**Figure 2.1B**). Protein extracts from these worms were applied for general western blotting detected by anti-GFP antibodies.

Both *pph-4.1* RNAi and empty RNAi vector treatments gave two bands: a lower band which is supposed to be DSB-1 at its predicted size and a higher band which is slow-migrating (**Figure 2.1C**). Furthermore, the upper band was more intense in the extracts from animals treated with *pph-4.1* RNAi compared to the animals treated with an empty vector.

To further examine if the slow-migrating band is due to phosphorylation, GFP-fused DSB-1 was purified by immunoprecipitation from *pph-4.1* RNAi treated worms. Then λ-phosphatase treatment was conducted on the immunoprecipitates before western blotting detection. A slow-migrating band appeared upon the expected size of GFP-DSB-1 in the sample without phosphatase treatment, while adding λ-phosphatase abolished it (**Figure 2.1D**). This result indicates the slow-migrating band is a phosphorylated form of DSB-1.

Taken together, these results suggest that protein DSB-1 is dephosphorylated in a PPH-4.1-dependent manner.

2.3.2 ATL-1^{ATR} kinase antagonizes PPH-4.1^{PP4} phosphatase to suppress DSB initiation

It is already known that DSB-1 is phosphorylated by ATM/ATR kinases. To investigate if ATM/ATR kinases antagonize PPH-4.1 phosphatase activity and thus regulate DSB levels in *C. elegans*, either *atm*^{ATM} or *atl-1*^{ATR} mutation was introduced into *pph-4.1(tm1598)* mutation background in order to make double mutants. DSB formation was examined in these double mutants through immunofluorescence and visualized by the staining of strand-invasion protein RAD-51. To quantify and compare RAD-51 focus number in different mutants at

different meiotic stages, a *C. elegans* hermaphrodite gonad was divided into 7 equally-sized zones (**Figure 2.2A**), and the number of RAD-51 foci was counted in each zone.

I found in mid-pachytene stage (zone 5), there were very few RAD-51 foci in *pph-4.1* mutants indicating few DSBs were formed in the absence of PPH-4.1, which is consistent with previous study (Sato-Carlton et al., 2014) (**Figure 2.2B and C**). Introducing *atm-1(gk186)* null mutation into *pph-4.1* background didn't change the DSB levels in mid-pachytene (**Figure 2.2B and C**). Given that *atl-1* homozygous mutants have severe mitotic defects due to replication errors (Garcia-Muse & Boulton, 2005), and there are numerous RAD-51 foci in the gonad of homozygous mutant (**Figure 2.3A**), I used an *atl*-1 heterozygous mutation (*atl-1/nT1*) to bypass these effects. However, I found that heterozygous mutation of *atl-1(tm853)* in *pph-4.1* mutants resulted in a significant increase of RAD-51 foci number suggesting a recovery of DSB formation. Moreover, *atl-1* heterozygous mutants alone led to an overall increase of DSB number when PPH-4.1 was present (**Figure 2.2B and C**). These extra DSBs resulting from the loss of ATL-1 in both wild type and *pph-4.1* background were not due to the mitotic DNA damage since the premeiotic region in *atl-1* heterozygous mutants don't have any RAD-51 signal which is the same as wild type animals (**Figure 2.3B**). Similarly, specifically depleting ATL-1 in meiosis by auxin-inducible degradation (AID) system also led to an increase of DSB number (**Figure 2.2B and C**). These data suggest that ATR kinase is opposing PPH-4.1 activity and acting to down regulate meiotic DSB formation in *C. elegans.*

ATM-1's contribution to DSB formation in meiosis was also investigated. In *C. elegans, atm-1* homozygous null mutants derived from heterozygous worms are as fertile as wild type animals, and the previous study has shown the DSB levels are only slightly changed in *atm-1* mutants (Li & Yanowitz, 2019). So in my work, meiotic DSB formation in the absence of *atm-1* was assessed in a more sensitive *rad-54(ok615)* background, in which RAD-51 protein cannot be removed from the recombination intermediates after DSBs are initiated (Mets & Meyer, 2009; Miyazaki et al., 2004). Compared to *rad-54* single mutants, deleting *atm-1* from *rad-54* background only led to a higher number of DSBs in late pachytene, while the RAD-51 foci appearance and disappearance showed a delayed kinetics in earlier stages (**Figure 2.3C**). This phenotype can be explained by the role of ATM-1 in timely loading of RAD-51 as previously reported (Li & Yanowitz, 2019).

Therefore, these results indicate that in *C. elegans,* ATR kinase rather than ATM plays an important role in antagonizing PPH-4.1 phosphatase in the aspect of regulating DSB formation.

2.3.3 DSB-1 possesses conserved ATM/ATR consensus motifs

It's well known that ATM/ATR kinases preferentially phosphorylate their substrates on SQ or TQ motifs (Traven & Heierhorst, 2005). I found DSB-1 also possesses five SQ motifs and based on the multiple sequence alignment of DSB-1 orthologs in different *Caenorhabditis* species (**Figure 2.4**), two out of these five sites are highly conserved. The existence of these SQ motifs strongly supports that DSB-1 may be dephosphorylated on these sites by PPH-4.1.

2.3.4 DSB-1 non-phosphorylatable mutants rescue the DSB formation defect and viability loss of PPH-4.1 deletion mutants

To further explore whether hyperphosphorylation of DSB-1 contributes to the reduction of meiotic DSBs in the absence of PPH-4.1, I generated *dsb-1(5A)*, a *dsb-1* non-phosphorylatable allele by CRISPR-Cas9 gene editing method, in which all the serines within the SQ sites were substituted with alanine; further, all the SQ sites are located within a predicted intrinsically disordered region, among which S137 and S186 are most highly conserved (**Figure 2.5A**). The mutants of *dsb-1(5A)* showed a comparable embryonic viability and male percentage to wild type animals (**Figure 2.5B**), indicating DSB-1 protein is still functional in this background.

Next, I examined the DSB formation when introducing this *dsb-1(5A)* mutation into both wild type and *pph-4.1* mutation background by RAD-51 staining. I found that *dsb-1(5A)* by its own has a high DSB number exceeding wild type level (**Figure 2.6A and B**), indicating phosphorylation of these five serines can limit the number of DSBs in wild type condition. Furthermore, compared to *pph-4.1* single mutants which hardly have DSBs, *pph-4.1; dsb-1(5A)* double mutants showed a significantly higher number of RAD-51 foci (**Figure 2.6A and B**), suggesting more DSB initiations in the double mutants. However, I observed a delay of RAD-51 foci peak in both *pph-4.1* single and *pph-4.1; dsb-1(5A)* double mutants (**Figure 2.6B**), and this delay also happened in *pph-4.1; atl-1/nT1* double mutants (**Figure 2.2C**). Since all strains where PPH-4.1 is absent show this phenotype, this reminds me about the previous studies on PP4 homologs in other organisms such as yeast and mammals, PP4 homologs are involved in the processing of somatic cell recombination intermediates including DSB resection and RAD-51 loading (J.-A. Kim et al., 2011; Lee et al., 2010; Villoria et al., 2019). Here in *C. elegans*, PPH-4.1 may also play a role in timely loading of RAD-51 in meiotic prophase.

In *C. elegans* hermaphrodites, low embryonic viability with a high incidence of males among the self-progeny always indicates a meiotic failure since male progeny is the product of X chromosome missegregation. I next scored the embryonic viability as well as male percentage of *pph-4.1; dsb-1(5A)* double mutants. In contrast to the low embryonic viability of *pph-4.1* single mutants (2%), *pph-4.1; dsb-1(5A)* double mutants showed a much higher embryonic viability which is up to 42% (**Figure 2.7A**). In addition, the frequency of males was largely reduced in *pph-4.1; dsb-1(5A)* double mutants compared to *pph-4.1* mutants itself (**Figure 2.7B**). Taken together, these results reveal that the PPH-4.1-dependent dephosphorylation of DSB-1 functions in promoting meiotic DSB formation in *C. elegans*.

2.3.5 DSB-1 non-phosphorylatable mutants rescue non-homologous pairing and synapsis of PPH-4.1 deletion mutants

The dramatic increase of embryonic viability in *pph-4.1;dsb-1(5A)* mutants is quite surprising since the previous studies on PPH-4.1 found that in *pph-4.1* mutants, the proper autosomal pairing and synapsis is largely reduced (Sato-Carlton et al., 2014); for example, the homologous pairing of chromosome V is no more than 25%, and assuming all the other autosomes possess the same pairing percentage, the expected probability of all five autosomes pair correctly is only 0.1%. This expectation is confirmed by the synapsis measurement and the bivalent numbers in diakinesis in *pph-4.1* single mutants. Wild type animals usually show six bivalents in diakinesis indicating the six paired chromosomes each of which is connected by chiasma, a physical link between the homologous chromosomes, while *pph-4.1* single mutants always exhibit less bivalents but univalents instead.

Therefore, I hypothesized that the increased DSB number in *pph-4.1; dsb-1(5A)* mutants may also raise the ratio of homologous pairing and thus promote the bivalent formation in the double mutants. To assess pairing, fluorescence in situ hybridization (FISH) was performed against 5S rDNA locus on chromosome V. Wild type animals showed paired 5S rDNA sites indicated by only one focus on each nucleus while a lot of nuclei from *pph-4.1* single mutants showed unpaired foci (**Figure 2.8A**). However, double mutants of *pph-4.1; dsb-1(5A)* showed a lot more paired foci (**Figure 2.8A**). In order to score the pairing percent throughout meiosis, a hermaphrodite gonad was divided into five equally-sized zones (**Figure 2.8B**). The quantitative analysis shows that *pph-4.1* single mutants only achieved 25% pairing as previous study showed (Sato-Carlton et al., 2014), but pairing was significantly increased to 70% in *pph-4.1; dsb-1(5A)* double mutants (**Figure 2.8C**).

Previous study has also shown that non-homologous synapsis including fold-back synapsis within a single chromosome and synapsis between non-homologous chromosomes occurs

in *pph-4.1* deletion mutants (Sato-Carlton et al., 2014). By immunofluorescence staining against protein ZIM-3, a marker of the pairing center on chromosome I and IV (Phillips & Dernburg, 2006); as well as the SC central region protein SYP-2 (**Figure 2.9A**), I found that *pph-4.*1 single mutants showed three or more ZIM-3 foci with SYP-2 stretches on a single nucleus, indicating the presence of non-homologous synapsis; while pph-*4.1; dsb-1(5A)* double mutants exhibit greater homologous synapsis (two ZIM-3 foci with SYP-2 stretches on each nucleus) (**Figure 2.9A**). To further investigate whether *dsb-1(5A)* mutation improves the homologous synapsis in *pph-4.1* background by changing the timing of synapsis, I did immunostaining against the SC central element SYP-2 and the SC axial element protein HTP-3 in entire gonads of wild type, *pph-4.1* single mutants and *pph-4.1; dsb-1(5A)* mutants. There is no difference in the timing of synapsis initiation and completion between these different genetic backgrounds (**Figure 2.9A**). A similar phenotype was observed in *pph-4.1; atl-1/nT1* mutants, increased DSBs induced by *atl-1* heterozygous mutation also led to an improvement of homologous synapsis in *pph-4.1* background (**Figure 2.9B**).

These findings are consistent with the recent studies that in *C. elegans*, synapsis prior to recombination is a dynamic state, in which the later time synapsis is stabilized by recombination (Liu et al., 2021; Machovina et al., 2016; Nadarajan et al., 2017; Pattabiraman et al., 2017; Roelens et al., 2015). Taken together, these results reveal that introducing DSBs into the pph-4.1 background also increases the fidelity of homologous pairing and synapsis.

2.3.6 DSB-1 non-phosphorylatable mutants rescue the chiasma formation failure in PPH-4.1 deletion mutants

To test whether the chiasma formation defect in *pph-4.1* mutants is rescued or not by *dsb-1(5A)* allele, I performed DAPI staining in diakinesis nuclei and scored nuclei with different numbers of bivalents and univalents in *pph-4.1; dsb-1(5A)* double mutants (**Figure 2.10A**). Unlike wild type worms in which nearly 100% diakinesis nuclei show six bivalents, most diakinesis nuclei in *pph-4.1* single mutants have univalents which were shown as more than six DAPI-stained bodies (**Figure 2.10A**). But in *pph-4.1; dsb-1(5A)* mutants, 47% of nuclei exhibit six DAPI-stained bodies corresponding to six bivalents, which is expected from the increase of homologous pairing in this double mutant.

To verify whether elevated DSB numbers are responsible for the rescue of chiasma formation in *pph-4.1; dsb-1(5A)* double mutants, the mutants of *pph-4.1* were irradiated by 50Gy γ-ray to introduce more DSBs into this background (performed by Peter Carlton) and the DAPI-stained bodies were scored after irradiation (**Figure 2.10B**). Compared to *pph-4.1*

control animals, 25% of diakinesis nuclei from the irradiated animals showed six bivalents, indicating a rescue of chiasma formation in these oocytes (**Figure 2.10B**). However, previous study showed that a lower dose of irradiation (10Gy) is sufficient to recover the bivalent in *spo-11* null mutants but not *pph-4.1* mutants (Dernburg et al., 1998; Sato-Carlton et al., 2014). The fact that *pph-4.1* single mutants need higher DSB number than *spo-11* mutants for bivalent formation is likely because of the involvement of PPH-4.1 in both timely processing of recombination intermediates and preventing non-homologous synapsis.

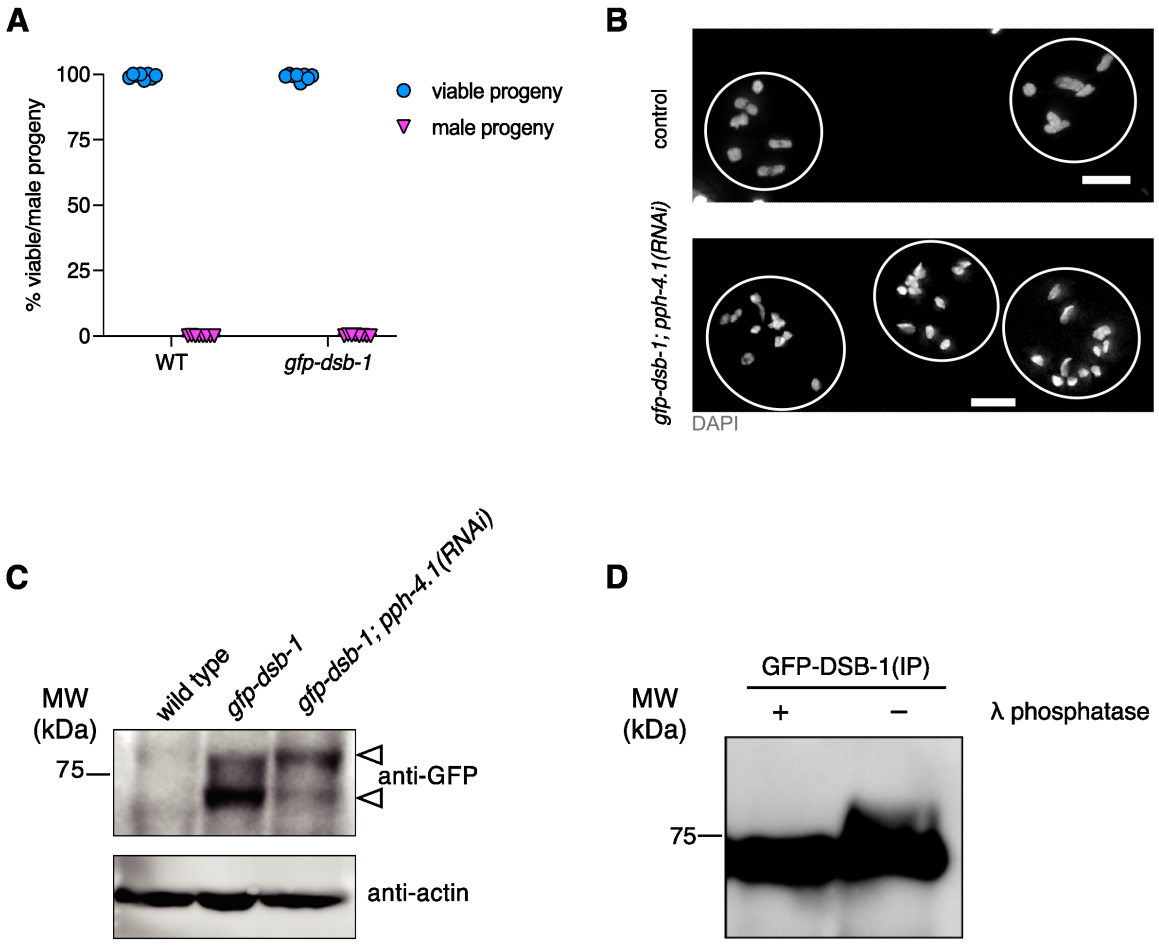

Figure 2.1 DSB-1 is dephosphorylated in a PPH-4.1^{PP4}-dependent manner. (A) Embryonic viability percentage and male progeny percentage of wild type animals and *gfp-dsb-1* mutants. Data points are from eight individual animals for each genotype. **(B)** Images of DAPI-stained diakinesis nuclei of control (N2) or *gfp-dsb-1* treated with *pph-4.1* RNAi (performed by Aya Sato-Carlton). The control nuclei contained 6 bivalents while the majority of nuclei contained univalents in *gfp-dsb-1; pph-4.1(RNAi)* animals. Scale bar, 5 μm. **(C)** Western blot of GFP-fused DSB-1 probed with α-GFP. GFP-DSB-1 detected in extracts from wild type and *gfp-dsb-1* worms (24 h post L4 stage) with either control RNAi or *pph-4.1* RNAi treatment (performed by Aya Sato-Carlton). A total protein amount of 97 μg was loaded in each lane. Arrowheads indicate two specific bands in the blot. Loading controls (α-actin) are shown at bottom. **(D)** Blot of GFP-DSB-1 purified by immunoprecipitation from young adult RNAi-treated worms with or without treatment with λ phosphatase (Protein extraction was performed by Aya Sato-Carlton).

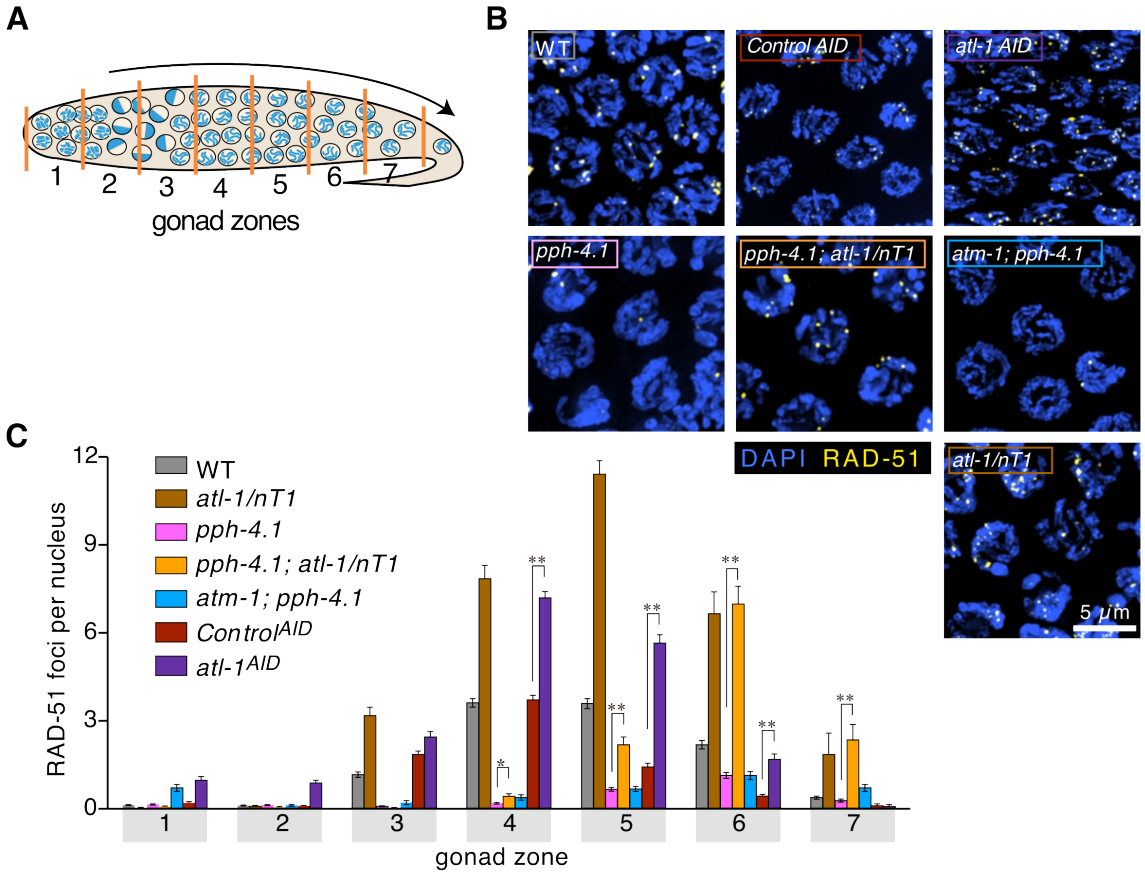

Figure 2.2 ATL-1^{ATR} kinase antagonizes PPH-4.1^{PP4} phosphatase on DSB initiation. (A) Schematic showing a hermaphrodite gonad divided into 7 equally-sized zones for RAD-51 focus scoring. **(B)** Immunofluorescence images of RAD-51 foci in mid-pachytene nuclei (zone 5) of the indicated genotypes (Staining of *atl-1^{AID}* and *control^{AID}* was performed by Liangyu Zhang; *atm-1(gk186); pph-4.1(tm1598)* staining was performed by Aya Sato-Carlton). Scale bar, 5 µm. **(C)** Quantification of RAD-51 foci in the germlines of the genotypes indicated in **(B)** (Quantification in *atm-1(gk186); pph-4.1(tm1598)* was performed by Aya Sato-Carlton). Seven gonads were scored for wild type and *pph-4.1(tm1598)*, three gonads were scored for *atl-1(tm853)/nT1, atl-1^{AID}*, *control^{AID}* as well as *pph-4.1(tm1598); atl-1(tm853)/nT1* double mutants, and four gonads were scored in *atm-1(gk186); pph-4.1(tm1598)*. The numbers of nuclei scored in zones 1-7 were as follows: for wild type, 420, 453, 377, 375, 345, 271, 296; for *pph-4.1(tm1598)*, 433, 423, 422, 413, 355, 322, 208; for *atl-1(tm853)/nT1*, 103, 137, 145, 115, 97, 75, 40; for *atl-1^{AID}*, 161, 193, 180, 241, 204, 117, 37; for *control^{AID}*, 143, 188, 233, 223, 192, 109, 28; for *pph-4.1(tm1598); atl-1(tm853)/nT1*, 126, 121, 98, 100, 94, 86, 49; for *atm-1(gk186);pph-4.1(tm1598),* 123, 153, 167, 140, 161, 156, 123. Significance was assessed via two-tailed *t* test, **P<0.01, ****P<0.0001.

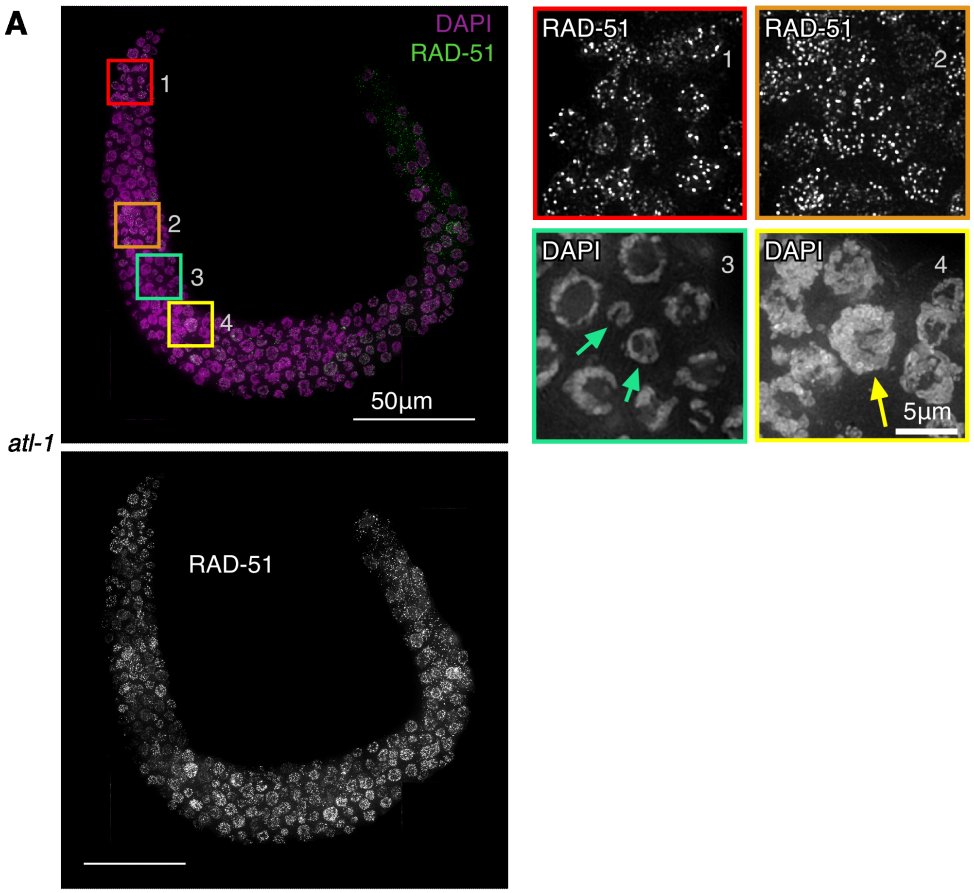

Figure 2.3 DSB formation in *atl-1* and *atm-1* mutants. (A) Maximum-intensity projection of an entire gonad arm from an *atl-1(tm853)* mutant (performed by Aya Sato-Carlton). Top left panel shows DAPI staining in magenta and RAD-51 staining in green. Bottom left panel shows RAD-51 foci in grayscale. Scale bar, 50 µm. Boxed insets on the top right show magnifications of the indicated color-matched regions highlighted on the left, which show numerous RAD-51 foci in both premeiotic and meiotic regions. Arrows indicate micronuclei resulting from improper mitotic division in box 3, and a large polyploid nucleus in box 4. Scale bar, 5 µm.

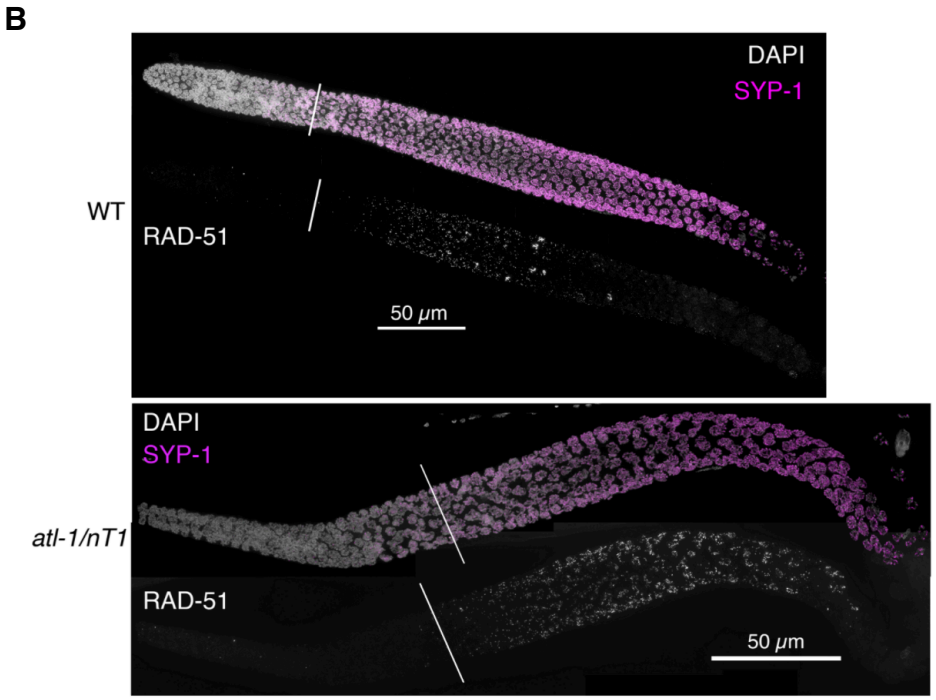

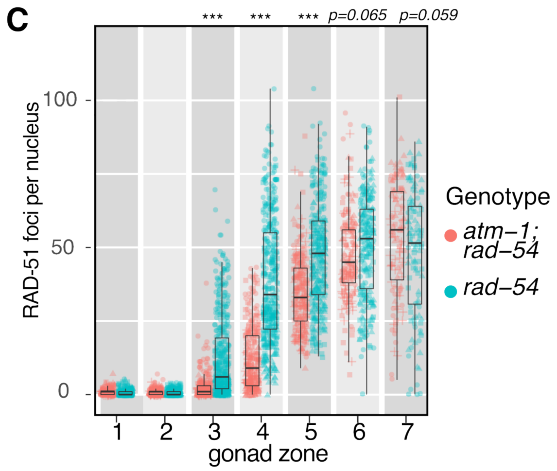

Figure 2.3 (B) ***Top*****:** Maximum-intensity projection of a wild type gonad. Above, DAPI staining is shown in grayscale and SYP-1, a component of the synaptonemal complex is shown in magenta. Below, RAD-51 is shown in grayscale. Diagonal line indicates the beginning of pachytene, before which few or no RAD-51 foci are seen. ***Bottom***: similar projection of a gonad from an *atl-1(tm853)/nT1* mutant. Scale bar, 50 μm. **(C)** Quantitation of RAD-51 foci in each of seven zones, compared between *rad-54* single mutants and *atm-1(tm853); rad-54* double mutants (performed by Aya Sato-Carlton). Four gonads were scored in *atm-1(tm853); rad-54* and three gonads were scored in *rad-54*; the numbers of nuclei scored in zone 1-7 were as follows: for *atm-1(tm853); rad-54*, 149, 218, 247, 281, 248, 181, 115; for *rad-54*, 253, 314, 444, 398, 312, 237, 112. Significance was assessed via two-tailed *t* test, ***P<0.001.

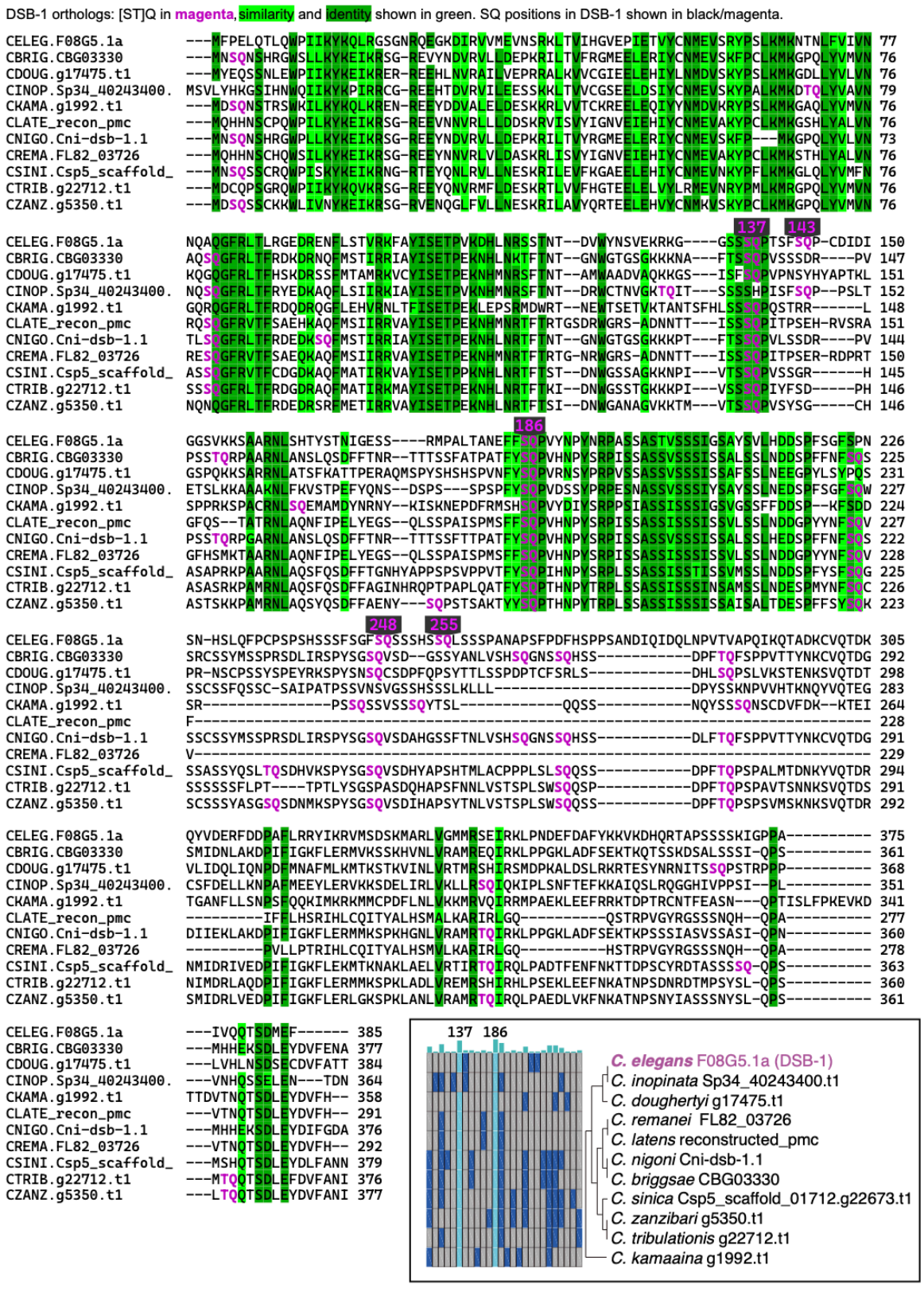

Figure 2.4 Sequence alignment of DSB-1 orthologs. Multiple sequence alignment (MSA) of DSB-1 orthologs in 11 Caenorhabditids (performed by Peter Carlton). [ST]Q sites are depicted in magenta. Similarity and identity are shown in shades of green. The five SQ sites of DSB-1 in *C. elegans* are highlighted in black. ***Right bottom***: all [ST]Q sites in the 11 species shown as a grid: sorted by their position from left to right in the alignment, dark blue indicates presence of an [ST]Q site shared by up to 9 species; cyan indicates a site shared by 10 or 11 species. Species and protein names are shown at right, along with an unrooted, unscaled phylogenetic tree to show relatedness of each species (Stevens et al., 2019).

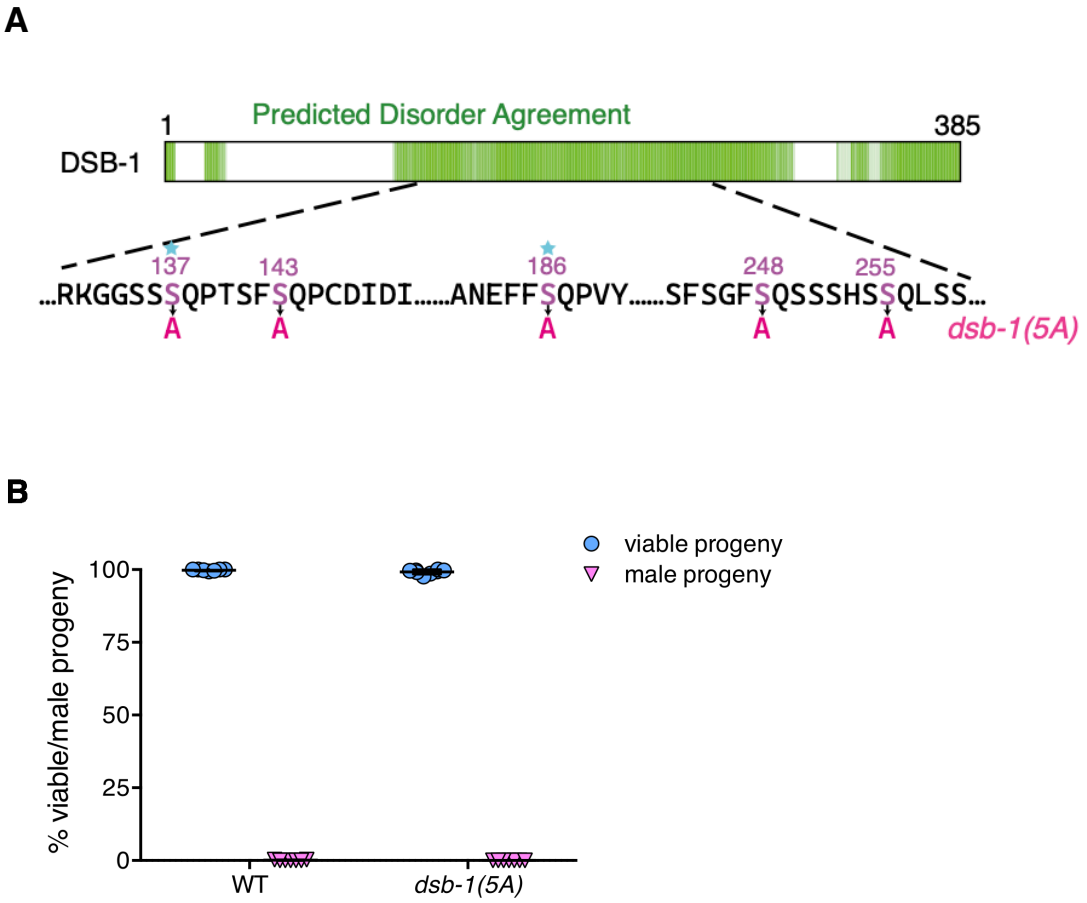

Figure 2.5 DSB-1 protein is functional in *dsb-1(5A)* mutants. (A) A schematic diagram of the DSB-1 protein sequence. Green regions indicate intrinsically disordered regions from the D^2P^2 database (Oates et al., 2012)**.** Five serines which were mutated into alanines in *dsb-1(5A)* within the SQ sites are shown in magenta, and sites conserved in 10 or more of the 11 Caenorhabditids in the *Elegans* group (see **Figure 2.4**) are indicated with a star. **(B)** Embryonic viability percentage and male progeny percentage of wild type animals and *dsb-1(5A)* mutants. Data points are from seven individual animals of wild type and eight individual animals of *dsb-1(5A)*.

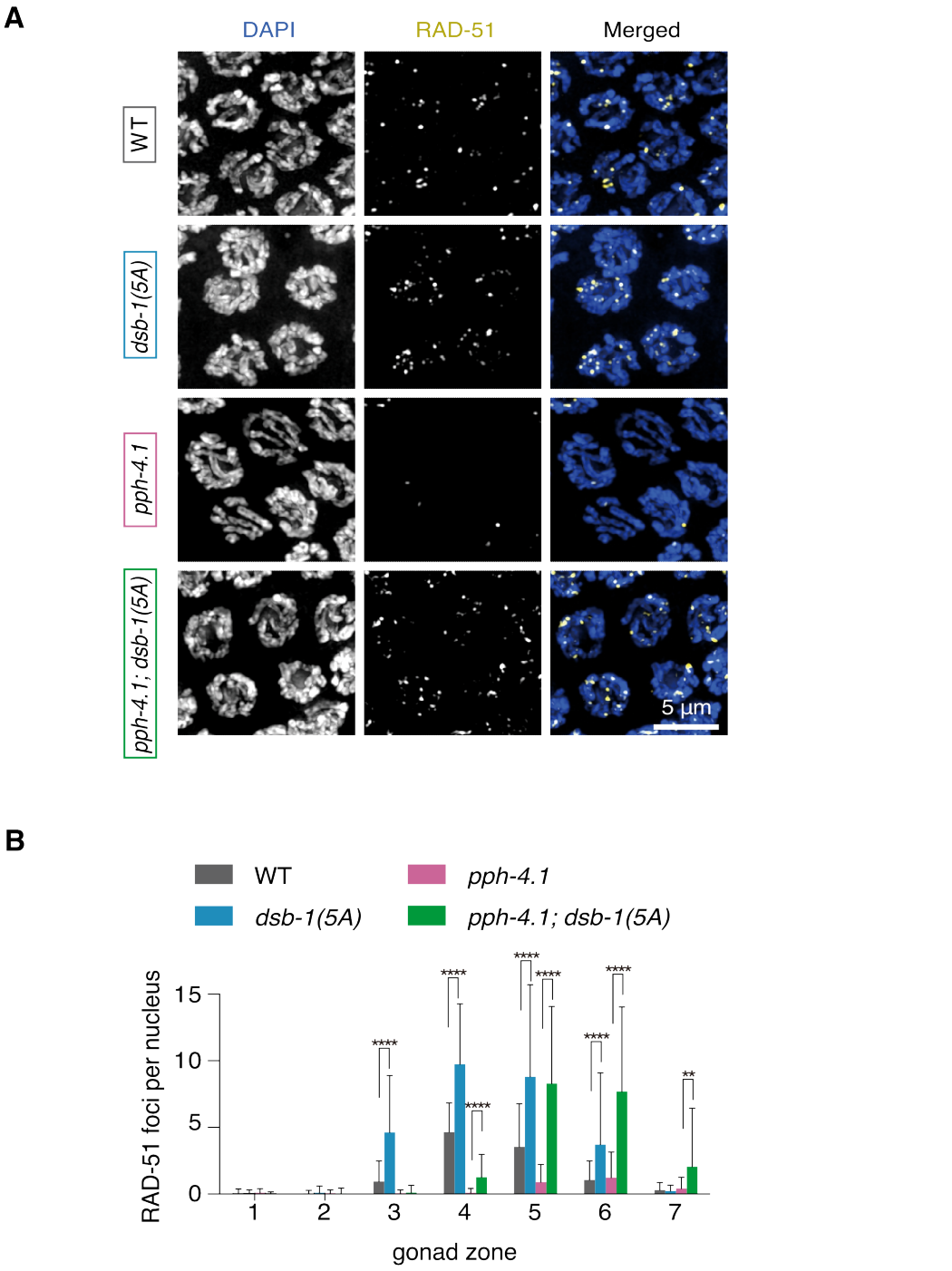

Figure 2.6 The *dsb-1(5A)* mutation rescues DSB formation defect of *pph-4.1* mutants. **(A)** Immunofluorescence images of RAD-51 foci in mid-pachytene nuclei of indicated genotypes. Scale bar, 5 µm. **(B)** Quantification of RAD-51 foci in the gonads of indicated genotypes in **(A)** (assisted by Minami Murai and Xuan Li). Four gonads were scored in each genotype; the numbers of nuclei scored in zone 1-7 were as follows: for wild type, 162, 201, 204, 230, 209, 155, 105; for *pph-4.1(tm1598)*, 145, 174, 201, 188, 167, 149, 74; for *dsb-1(5A)*, 175, 220, 197, 163, 143, 116, 90; for *pph-4.1(tm1598); dsb-1(5A)*, 171, 152, 121, 180, 185, 137, 85. Significance were assessed via the two-tailed *t* tests, **P<0.01, ****P<0.0001.

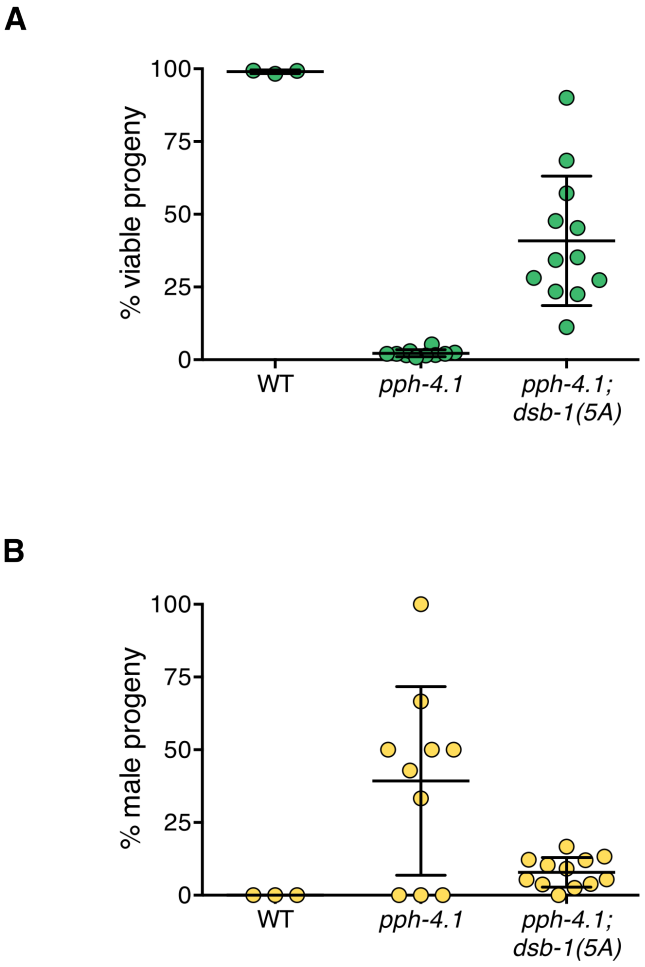

Figure 2.7 The *dsb-1(5A)* mutation rescues viability loss of *pph-4.1* mutants. (A) Embryonic viability percentage of the indicated genotypes. **(B)** Male progeny percentage indicating the rate of X chromosome nondisjunction during meiosis in wild type, *pph-4.1(tm1598)* and *pph-4.1(tm1598); dsb-1(5A)* mutants. (A and B were assisted by Xuan Li). Data points in **(A)** and **(B)** are from three individual animals of wild type, ten individual animals of *pph-4.1(tm1598)* and twelve individual animals of *pph-4.1(tm1598); dsb-1(5A)*.

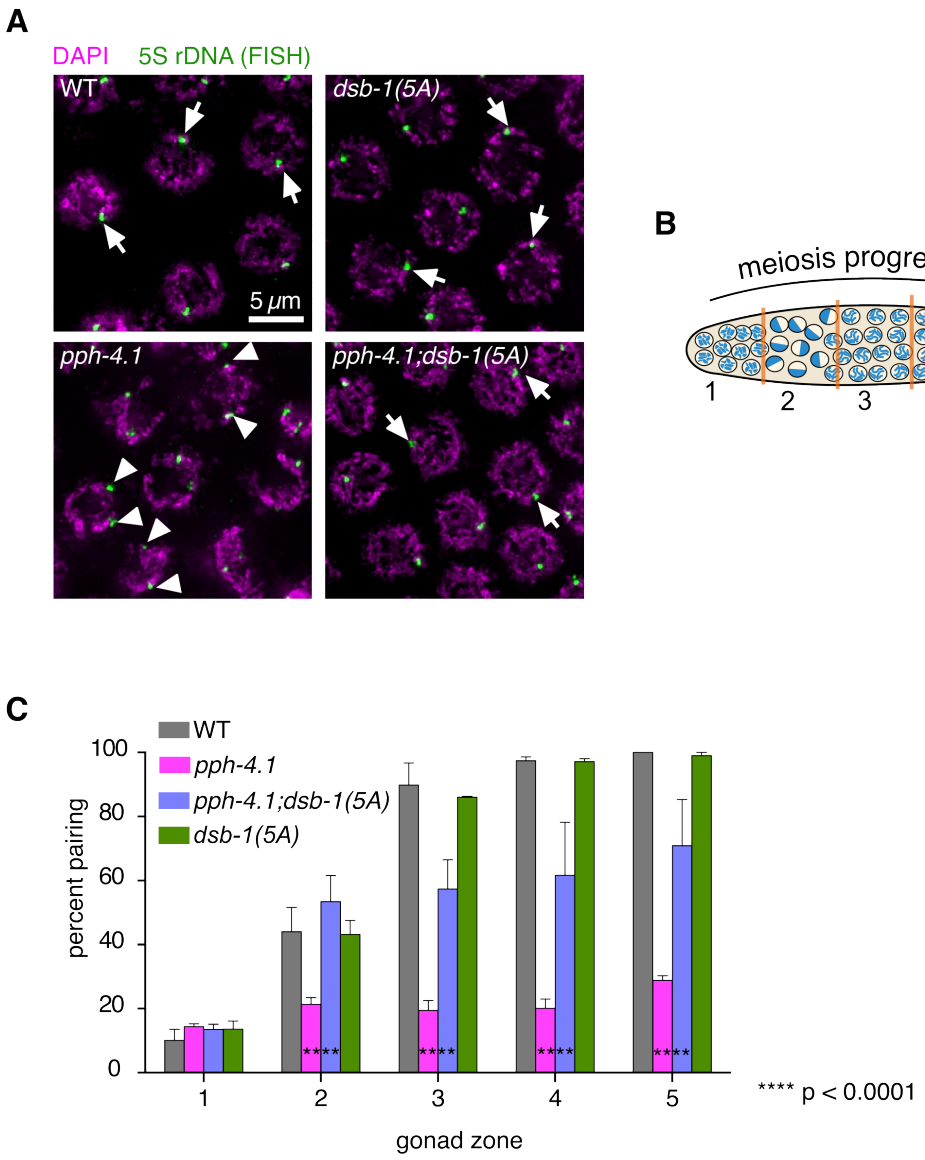

Figure 2.8 Homologous pairing defects are partially rescued by the *dsb-1(5A)* allele in *pph-4.1* mutants. (A) FISH images show paired 5S rDNA sites in wild type and *pph-4.1(tm1598); dsb-1(5A)* worms (left top and right bottom; arrowheads indicate paired foci), and unpaired sites in *pph-4.1(tm1598)* mutants (left bottom; arrows indicate unpaired foci) at pachytene (assisted by Masaaki Shimazoe). Scale bar, 5 μm. **(B)** Schematic showing a hermaphrodite gonad divided into 5 equally-sized zones for FISH focus scoring. **(C)** Quantification of pairing for chromosome V shown as the percent of nuclei with paired signals in each zone (assisted by Xuan Li). Four gonads were scored for each genotype. The total number of nuclei scored for zone 1-5 respectively was as follows: for wild type, 163, 266, 208, 148, 76; for *pph-4.1(tm1598)*, 300, 283, 257, 219, 124; for *pph-4.1(tm1598); dsb-1(5A),* 335, 318, 266, 224, 137. Significance was assessed by chi-squared test for independence, ****P<0.0001.

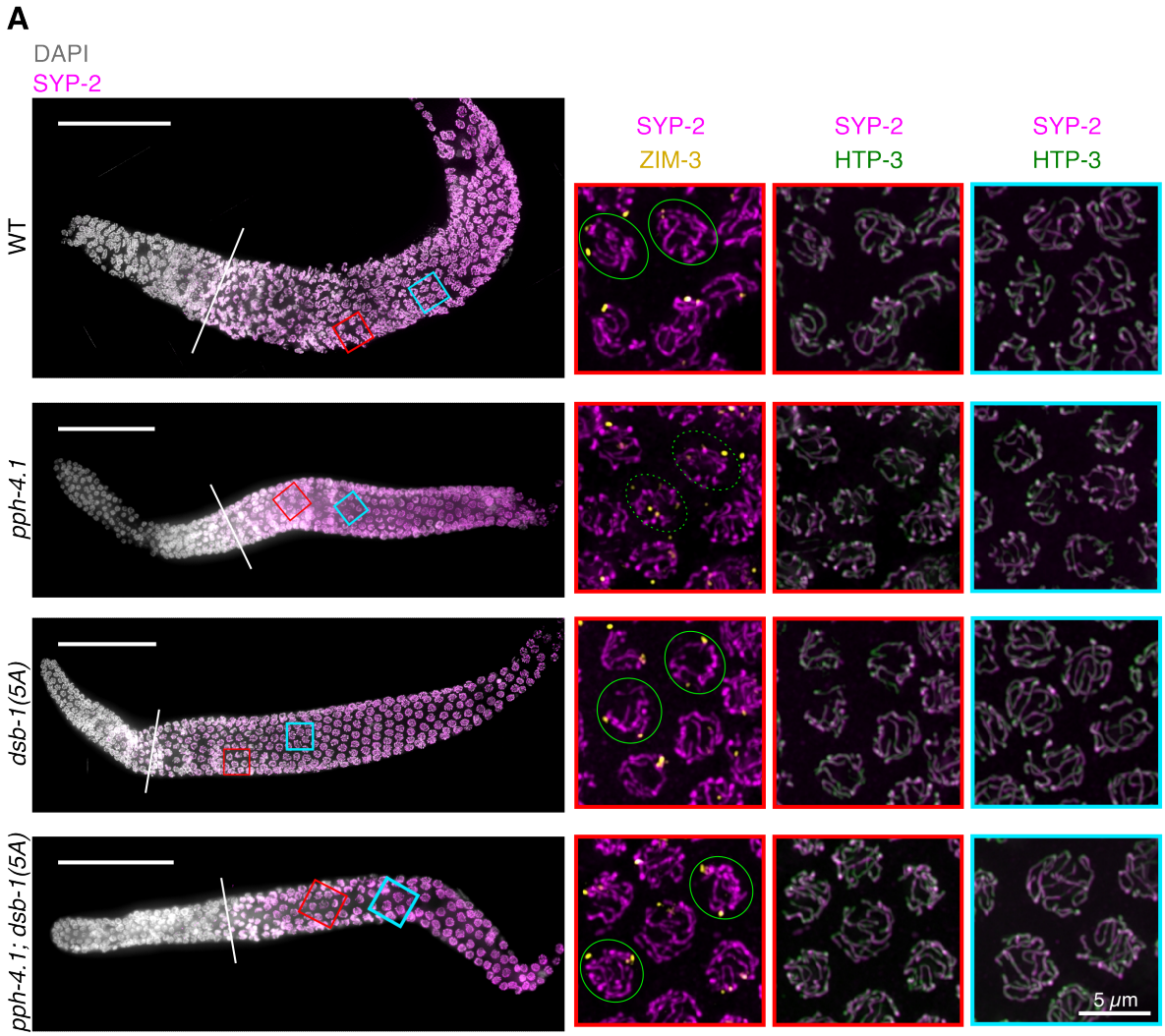

Figure 2.9 Homologous synapsis is improved by *dsb-1(5A)* allele in *pph-4.*1 mutants.
(A) Immunofluorescence images of wild type, *pph-4.1 (tm1598)*, *dsb-1(5A)* and *pph-4.1(tm1598); dsb-1(5A)* mutants. Left panel shows the maximum-intensity projection of a gonad arm from the premeiotic region to late pachytene of each indicated genotype. DAPI staining is shown in grayscale and SYP-2, a central element of the synaptonemal complex, is shown in magenta. Diagonal line indicates the leptotene/zygotene transition zone where synapsis begins. Scale bar, 50 μm. Boxed insets on the right show the magnifications of the nuclei in the indicated color-matched regions highlighted on the left. ZIM-3 staining, detecting the pairing centers of chromosome I (right end) and IV (left end) is shown in yellow; HTP-3, an axial element protein is shown in green and SYP-2 staining is shown in magenta. After homologous pairing and synapsis, two ZIM-3 foci per nucleus are expected to be seen. Green circles show examples of three ZIM-3 foci per nucleus, each connected to SYP-2 stretches, in *pph-4.1(tm1598)* single mutants, indicating non-homologous synapsis; while double mutants of *pph-4.1(tm1598)*; *dsb-1(5A)* show increased number of homologously paired ZIM-3 foci (2 foci per nucleus, shown in green circle), indicating rescued homologous synapsis. Complete colocalization of HTP-3 and SYP-2 indicates the fully synapsed chromosomes in each genotype. Scale bar, 5 μm.

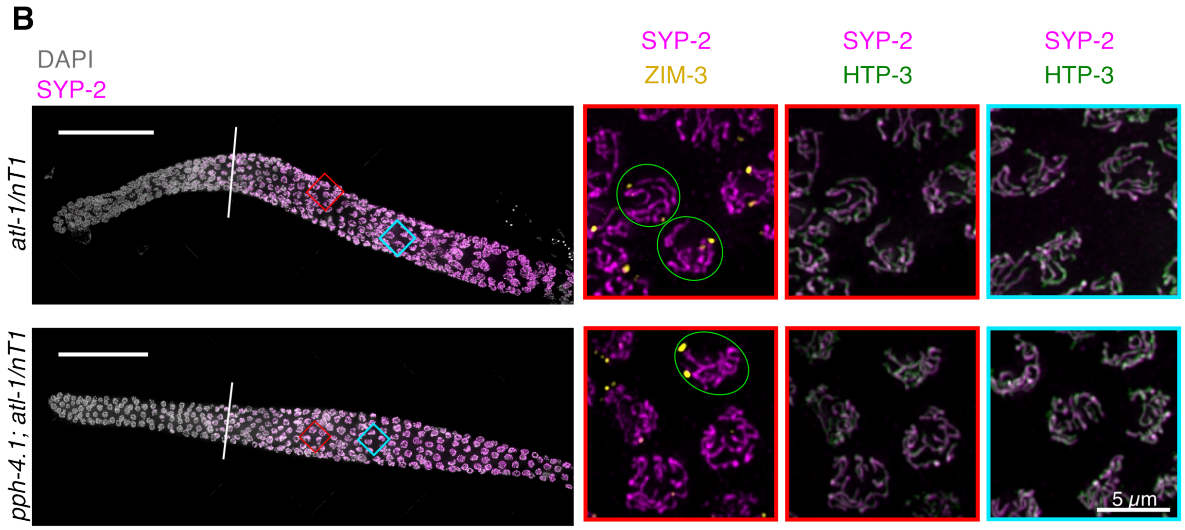

Figure 2.9 (B) Immunofluorescence images showing synapsis in *atl-1/*nT1 and *pph-4.1; atl-1/nT1* mutants. Left panel shows the maximum-intensity projection of a gonad arm from the premeiotic region to late pachytene of each indicated genotype. DAPI staining is shown in grayscale and SYP-2 is shown in magenta. Diagonal line indicates the leptotene/zygotene transition zone where synapsis begins. Scale bar, 50 μm. Boxed insets on the right show the magnifications of the nuclei in the indicated color-matched regions highlighted on the left. ZIM-3 staining is shown in yellow, HTP-3 is shown in green, and SYP-2 is shown in magenta. Scale bar, 5 μm.

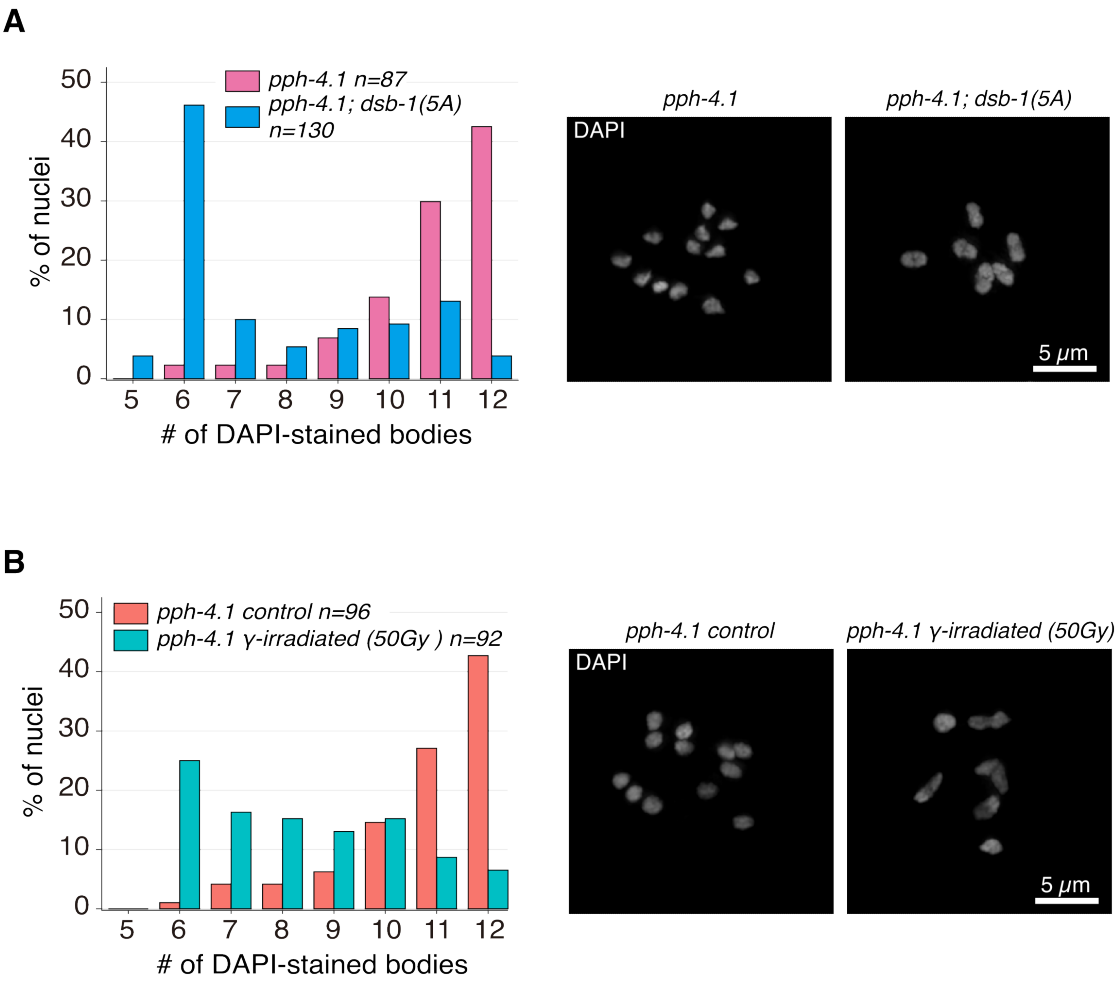

Figure 2.10 Chiasma formation is partially rescued by *dsb-1(5A)* allele in *pph-4.1* mutants. **(A)** ***Left:*** the number of DAPI-stained bodies shown as percentages of the indicated number of diakinesis oocyte nuclei scored for *pph-4.1(tm1598)* and *pph-4.1(tm1598); dsb-1(5A)* mutants. The numbers of nuclei scored for each genotype were: 87 for *pph-4.1(tm1598)*, 130 for *pph-4.1(tm1598); dsb-1(5A).* ***Right:*** images of DAPI-stained diakinesis nuclei in a *pph-4.1(tm1598)* mutant and a *pph-4.1(tm1598); dsb-1(5A)* double mutant. Scale bar, 5 µm. **(B)** ***Left:*** the number of DAPI-stained bodies shown as percentages of the indicated number of diakinesis oocyte nuclei scored in *pph-4.1(tm1598)* mutants with or without γ-irradiation. The numbers of nuclei scored for each genotype were: 96 for *pph-4.1(tm1598) control*, 92 for *pph-4.1(tm1598) γ-irradiated (50Gy).* ***Right:*** images of DAPI-stained diakinesis nuclei in a *pph-4.1(tm1598) control* animal and a *pph-4.1(tm1598)* mutant exposed to 50Gy of γ-irradiation. Scale bar, 5 µm.

Chapter 3

DSB-1 phosphorylation functional analysis and its relationship with DSB-2

3.1 Introduction

DSB-2 is a paralog of DSB-1 in many species of *Caenorhabditis*. In *C. elegans*, DSB-2 has been identified to be required for efficient DSB formation during meiosis (Rosu et al., 2013). However, the meiotic defects in *dsb-2* null mutants are less severe compared to *dsb-1* null mutants. Unlike the complete lack of DSB formation and extremely low embryonic viability when DSB-1 is absent, *dsb-2* null mutants are still capable of forming a small number of DSBs, and the embryonic viability is also higher than *dsb-1* null mutants, suggesting DSB-2 plays a less important role than DSB-1 in DSB formation. Furthermore, it has been found that in *dsb-2* null mutants, the crossover formation defects resulting from the profound reduction of DSBs aggravate with age, leading to an even lower embryonic viability and higher male frequency in old animals compared to young adults (Rosu et al., 2013). Additionally, DSB-3 has also been identified as a DSB-promoting protein in *C. elegans* and according to recent study, DSB-3 is a homolog of MEI4 and potentially interacts with DSB-1 (Hinman et al., 2021b).

Here I describe the functional analysis of DSB-1 phosphorylation in the absence of DSB-2 and gain insight into the relationship between DSB-1 and DSB-2. I show the evidence that the high levels of DSBs induced by blocking DSB-1 phosphorylation is independent of DSB-2. The meiotic defects in *dsb-2* null mutants are attributed to both a reduction of DSB-1 protein amount and an increase of DSB-1 phosphorylation level. When DSB-2 is present, the age-dependent increase of DSB-1 phosphorylation is likely to contribute to the poor DSB production in aged animals. Moreover, DSB-1, DSB-2 and DSB-3 are predicted to form a complex which may facilitate the DSB initiation during meiosis.

3.2 Materials and methods

3.2.1 *C. elegans* strains

Worm strains were maintained at 20 °C on nematode growth medium (NGM) plates seeded with OP50 bacteria under standard conditions (Brenner, 1974). Bristol N2 was used as the wild type strain and all mutants were derived from an N2 background. Strains used in this study are shown as below:

- PMC575 *icm97 [gfp-dsb-1](IV)*
- PMC569 *icm98 [dsb-1(S137A_S143A_S186A_S248A_S255A)](IV)*
- OC271 *pph-4.1(tm1598)/hT2[bli-4(e937) let-?(q782) qIs48](I;III)*
- PMC583 *pph-4.1(tm1598)/hT2[bli-4(e937) let-?(q782) qIs48](I;III); icm97 [gfp-dsb-1](IV)*

- PMC537 *icm111 [dsb-1(S137A_S143A)](IV)*
- PMC551 *icm112 [dsb-1(S186A)](IV)*
- PMC552 *icm113 [dsb-1(S137A_S143A_S186A)](IV)*
- PMC670 *icm114 [gfp-dsb-1(S137A_S143A_S186A_S248A_S255A)](IV)*
- AV477 *dsb-2(me96) (II)*
- PMC634 *pph-4.1(tm1598)/hT2[bli-4(e937) let-?(q782) qIs48](I;III); icm112 [dsb-1(S186A)](IV)*
- PMC630 *dsb-2(me96) (II); icm111 [dsb-1(S137A_S143A)](IV)*
- PMC631 *dsb-2(me96) (II); icm112 [dsb-1(S186A)](IV)*
- PMC603 *dsb-2(me96) (II); icm113 [dsb-1(S137A_S143A_S186A)](IV)*
- PMC580 *dsb-2(me96) (II); icm98 [dsb-1(S137A_S143A_S186A_S248A_S255A)](IV)*
- PMC637 *icm97 [gfp-dsb-1](IV);dsb-2(me96) (II)*
- PMC636 *icm114[gfp-dsb-1(S137A_S143A_S186A_S248A_S255A)](IV); dsb-2(me96) (II)*

3.2.2 Generation of mutants via CRISPR-Cas9 genome editing system

A series of dsb-1 non-phosphorylatable mutants were generated by CRISPR-Cas9 genome editing assay as described in Chapter 2 (*dsb-1(1A)* and *dsb-1(3A)* mutants were constructed by Jacky Tam). A list of oligonucleotides used is provided as below:

- *dsb-1(S137A_S143A)* CRISPR crRNA1: 5'-CAACAGTGTCGAGAAACGGA-3'
- *dsb-1(S137A_S143A)* CRISPR crRNA2: 5'-AATATCGCATGGTTGGGAGA-3'
- *dsb-1(S186A)* CRISPR crRNA1: 5'-CAGTCTACAATCCTTACAAT-3'
- *dsb-1(S186A)* CRISPR crRNA2: 5'-TGCTGTGAGTGCTGGCATCC-3'
- *dsb-1(S137A_S143A)* homology template for CRISPR: 5'-GTTGGTGGAATACGTATGTGATAAGTTTCTTGCCGCGGATTTCTTCACCGAGCCACCAATATCgATgTCGCATGGcTGaGcGAAaGATGTCGGCTGaGcgGAgGAaCCaCCtTTaCGcTTtTCaACggaGTTGTACCACACATctataattcaaaaatgaaacttgaaactattaaaagaataaagaatacCGGTATTTG-3'
- *dsb-1(S186A)* homology template for CRISPR: 5'-GTGAATCATCGTGGAGAACGCTGTAAGCCGAGCCAATCGATGAACTAACAGTGCTGGCACTCGAgGCTGGaCggTTGTAtGGgTTGTAaACTGGCTGaGcaAAaAAcTCgTTaGCgGTaAGaGCTGGCATaCGaGAACTTTCACCAATGTTGGTGGAATACGTATGTGATAAGTTTCTTGCCGCGGATTTCTTCACCGAG-3'
- *dsb-1(S137A_S143A)* genotyping forward primer: 5'-GCGTAAAGGTGGTTCCTCCG-3'
- *dsb-1(S137A_S143A)* genotyping reverse primer: 5'-GGAGAACGCTGTAAGCCGAG-3'

- *dsb-1(S186A)* genotyping forward primer: 5'-GTATGCCAGCTCTTACCGCT-3'
- *dsb-1(S186A)* genotyping reverse primer: 5'-AAATGAAGGTGCGTTTGCGG-3'

3.2.3 Immunofluorescence and cytological analysis

Immunostaining, imaging as well as quantification analysis were performed as described in Chapter 2.

3.2.4 Embryonic viability scoring

The embryonic viability and male progeny of each genotype were scored as described in Chapter 2. Hermaphrodites start to lay eggs after they transition from L4 to adult, and lay most eggs in the first three days. To detect the aging effect, the embryonic viability and male percentage in the first three days were analyzed individually.

3.2.5 Lysate preparation and western blotting

To prepare samples for general western blotting of GFP-fused DSB-1, 24 h post-L4 stage 72 h post-L4 stage worms were collected in M9 + 0.01% Tween buffer, washed three times with M9 buffer and then frozen in -80 °C. Frozen worm pellet was suspended in urea lysis buffer (20 mM HEPES pH 8.0, 9M Urea, 1 mM sodium orthovanadate), sonicated (Taitec VP505 homogenizer; 50% output power, cycle of 10 sec on and 10 sec off for 7 min total) and spun down at 16000 g at 4 °C for 15 min. The supernatant was used to measure protein concentration using the BCA kit (Pierce BCA protein assay kit #23225; Thermo Scientific), and a total protein amount of 97 µg or 162 µg was loaded for western blotting after boiling for 10 min in SDS-PAGE sample buffer. Western blotting was performed as described in Chapter 2.

3.2.6 Alpha Fold structure prediction

Predictions were generated using the ColabFold interface (github.com/sokrypton/ColabFold, commit ebf4df8) to the AlphaFold2 pipeline on the Colab platform (Google Research). Predictions were run on trimers using protein sequences for DSB-1, DSB-2, DSB-3 (*C. elegans* and *C. inopinata*) retrieved from Wormbase (Davis et al., 2022), and Rec114 and Mei4 (*Homo sapiens* and *Saccharomyces cerevisiae*) retrieved from Uniprot (UniProt Consortium, 2021).

3.3 Results

3.3.1 DSB-1 non-phosphorylatable mutants rescue the DSB and crossover formation defects resulting from the absence of DSB-2

In *C. elegans* and other species of Caenorhabditis genus, *dsb-2*, which is a paralog of *dsb-1* is also required specifically to promote the DSB formation of meiotic recombination. In *C. elegans,* the loss of DSB-2 causes a reduction of DSB formation, which in turn leads to a failure in chiasma/crossover formation and thus embryonic inviability. Furthermore, these meiotic defects become more severe with advancing maternal age (Rosu et al., 2013). Although there is a significant reduction of DSB formation in *dsb-2* null mutants, the DSBs are not eliminated, which indicates that without DSB-2, DSB-1 is still sufficient to initiate DSBs but the activity of DSB-1 is lower compared to when DSB-2 is present.

To examine whether *dsb-1(5A)* mutation is dependent on DSB-2 to exert its ability in DSB regulation, I checked the DSB formation in *dsb-1(5A); dsb-2(me96)* double mutants by RAD-51 staining. Consistent with previous research, *dsb-2* single mutants show a very low number of DSBs (Rosu et al., 2013), whereas this number dramatically increased in *dsb-1(5A); dsb-2* double mutants (**Figure 3.1A and B**). Moreover, the overall number of meiotic DSBs in the double mutants is at a similar level as the dsb-1*(5A)* mutant its own (**Figure 3.1B**), which suggests that the high levels of DSB formation in *dsb-1(5A)* mutants is completely independent of *dsb-2.*

In addition, I also tested the crossover formation in *dsb-1(5A); dsb-2* mutants by DAPI staining. Compared to *dsb-2* single mutants which always exhibit a mixture of bivalents and univalents in diakinesis oocytes, most of the *dsb-1(5A); dsb-2* double mutants show six bivalents as wild type animals, indicating a normal formation of crossover (**Figure 3.2A and B**) and which in turn leads to a full rescue of the embryonic inviability in *dsb-2* background (**Figure 3.2C**).

3.3.2 Serine 186 accounts most for the meiotic defects when DSB-2 is absent

In order to gain a deeper understanding of the five SQ sites, I constructed a series of *dsb-1* non-phosphorylatable mutants in which one or more serines within the SQ motifs were mutated into alanine: *dsb-1(S186A)*, which is *dsb-1(1A)* for short; *dsb-1(S137A_S143A)*, which is *dsb-1(2A)* for short and *dsb-1(S137A_S143A_S186A)*, which is *dsb-1(3A)* for short (**Figure 3.3A**). All these mutants exhibit a wild-type level of embryonic viability indicating DSB-1 protein is functional (**Table 3.1**).

To find out if these *dsb-1* non-phosphorylatable alleles can rescue *dsb-2* mutant's meiotic defects, I combined *dsb-2* mutation with each *dsb-1* non-phosphorylatable mutation and made different double mutants. Through embryonic viability and male progeny score, I found all these *dsb-1* non-phosphorylatable alleles rescued embryonic inviability and high incidence of males in *dsb-2* background to some extent (**Table 3.1**). Furthermore, *dsb-1(1A)* and *dsb-1(3A)* mutations which cover the S186A substitution even led to a full recovery of embryonic viability and male frequency in *dsb-2* mutants (**Table 3.1**). Given that the meiotic defects worsen with age in *dsb-2* mutants, I also analyzed the viable and male progeny produced by the double mutants on each day, and I found that *dsb-1(1A)* and *dsb-1(3A)* rescued the embryonic viability and male frequency in *dsb-2* background to wild type levels at all maternal ages (**Figure 3.3B and C**). On the other hand, *dsb-1(2A)* which does not contain the S186A substitution rescued these defects completely only in young age animals (day 1 post-L4 stage) but showed far less rescue of older animals (day 3 post-L4) (**Figure 3.3B and C**). Together, these results suggest that the DSB-promoting activity of DSB-1 is slowed down by phosphorylation on any of these SQ sites, and S186 is likely to act as a main factor determining the reduced DSB activity in aged animals when DSB-2 is absent. Moreover, quantitative analysis of DSB levels by RAD-51 staining and quantification in *dsb-1(1A)*, *dsb-1(2A)*, *dsb-1(3A)* and *dsb-1(5A)* mutants showed that the mutants containing S186A substitution exhibited a greater number of DSBs than wild type animals either in early stage (for *dsb-1(1A)* and *dsb-1(3A)*) or throughout the meiotic prophase (for *dsb-1(5A)*) (**Figure 3.4**). I also observed an overall higher DSBs level in *dsb-1(5A)* mutants compared to *dsb-1(3A)* mutants, suggesting the phosphorylation on the other two SQ sites (S248 and S255) specifically in *dsb-1(5A)* also contributes to down-regulating the DSB formation (**Figure 3.4**).

Although *dsb-1(1A)* allele is sufficient to rescue *dsb-2* mutant defects, it doesn't suffice to fully rescue the defects in *pph-4.1* background. The embryonic viability is only slightly increased in *pph-4.1; dsb-1(1A)* double mutants (**Table 3.1; Figure 3.5A**). RAD-51 staining revealed that compared to wild type animals, the DSB levels in *dsb-1(1A)* mutants increased mildly; introducing *dsb-1(1A)* mutation into *dsb-2* and *pph-4.1* background both resulted in an increased number of DSBs compared to respective single mutant, *pph-4.1* and *dsb-2* (**Figure 3.5B and C**). One explanation to the difference of embryonic viability between *dsb-2; dsb-1(1A)* and *pph-4.1; dsb-1(1A)* mutants could be that the requirement of DSB numbers is higher in *pph-4.1* background for the conversion from DSBs to COs than in *dsb-2* background, which is due to the involvement of PPH-4.1 in multiple meiotic stages and is also in agreement with the prior observation that higher dose of irradiation was required for the bivalent formation in *pph-4.1* mutants.

3.3.3 Age-dependent DSB-1 phosphorylation contributes to the reduction of DSB initiation activity in presence of DSB-2

People have already found that in *C. elegans*, DSB initiation activity is reduced in older animals compared to younger animals (Raices et al., 2021; Sato-Carlton et al., 2014). To investigate whether DSB-1 phosphorylation is increased with age and thus leads to the reduction of DSB initiation activity in older animals, western blotting was performed in young (24 h post-L4 stage) and old (72h post-L4 stage) adult animals in different genetic backgrounds to assess DSB-1 phosphorylation levels.

In *gfp-dsb-1* worms, the proportion of the slow-migrating band was increased in old animals, indicating a higher level of DSB-1 phosphorylation in aged animals (**Figure 3.6**). In the dsb-2 background, there was an overall reduction of DSB-1 protein amount compared to *gfp-dsb-1* (control) animals, which is consistent with previous studies (Stamper et al., 2013). Furthermore, in young animals, the proportion of the slow-migrating band was higher in *dsb-2* mutants than *gfp-dsb-1* worms (**Figure 3.6**), which means it's likely that both the reduced protein amount and increased protein phosphorylation of DSB-1 contribute to the low DSB activity in *dsb-2* young adults. However, there was no significant difference in the phosphorylated DSB-1 ratio between young and old *dsb-2* animals, which was further verified by loading more protein in western blotting (**Figure 3.6**). One explanation could be that there may be some factors other than DSB-1 phosphorylation responsible for the age-dependent meiotic DSB reduction in *dsb-2* mutants. Another explanation is that the phosphorylation specific on S186 of DSB-1 is elevated in *dsb-2* old animals, but it is not detectable without the antibody against phospho-S186. I attempted to generate this phospho-specific antibody but failed to detect any relevant signal.

In addition, DSB-1 phosphorylation was largely reduced in *dsb-1(5A)* mutants since the slow-migrating band was very weak in both young and old animals. However, a smearing of GFP-DSB-1(5A) was still detected above the main band; because DSB-1 protein contains 91 serine, threonine or tyrosine residues in the length of 385 amino acids, this smearing suggests that DSB-1 may be also phosphorylated on such sites other than the five SQ motifs.

3.3.4 DSB-1 is predicted to form a heterotrimeric complex with DSB-2 and DSB-3

DSB-3 has been recently identified as an ortholog of Mei4 in nematodes, and it is likely to participate in a heterotrimeric complex with DSB-1 and DSB-2 (Hinman et al., 2021b) similar to Rec114-Rec114-Mei4 ternary complex shown to exist in budding yeast (Claeys Bouuaert

et al., 2021). In the analysis on the predicted structural properties of such a complex via the structure prediction pipeline known as AlphaFold (Jumper et al., 2021; Mirdita, Schütze, et al., 2021), three possible complexes were tested: (1) A heterotrimer containing one copy of DSB-1, DSB-2 and DSB-3 respectively. (2) A complex containing two copies of DSB-1 and one copy of DSB-3. (3) A complex containing two copies of DSB-2 and one copy of DSB-3.

In the predicted DSB-1:DSB-2:DSB-3 complex, the alpha-helical C-termini of DSB-1 and DSB-2 wrap around one another, forming a channel that the helical N-terminus of DSB-3 goes through in it (**Figure 3.7**). Moreover, a prediction for the orthologs of DSB-1, DSB-2 and DSB-3 in *Caenorhabditis inopinata* gave the same result and a similar structure was predicted for the human and yeast Rec114-Mei4 complexes in 2:1 in stoichiometry (**Figure 3.7**). It appears that all of these structural predictions are consistent with models based upon yeast two-hybrid (Hinman et al., 2021b; Maleki et al., 2007) and cross-link mass spectrometry analysis (Claeys Bouuaert et al., 2021). However, this prediction was not found in the DSB-2:DSB-2:DSB-3 models but three out of five DSB-1:DSB-1:DSB-3 models, which suggests a DSB-1:DSB-1:DSB-3 complex may be more likely to form than a DSB-2:DSB-2:DSB-3 complex. This is also in agreement with the two yeast-hybrid result showing that it is DSB-1 but not DSB-2 binding to DSB-3 directly (Hinman et al., 2021b). Furthermore, this result can also explain the stronger phenotype when losing DSB-1 than losing DSB-2.

Surprisingly, none of the five SQ sites in DSB-1 are involved in the interacting regions based on the predictions, which means the phosphorylation of DSB-1 may not contribute to the protein binding in the complex.

Genotype	Embryonic viability (%)	Male percentage (%)	Total # eggs scored
WT	99.28	0.04	1990
dsb-1(1A)	98.47	0.15	3427
dsb-1(2A)	98.25	0.00	1347
dsb-1(3A)	99.29	0.19	2056
dsb-1(5A)	99.22	0.00	2546
pph-4.1(tm1598)	2.00	45.60	1424
dsb-2(me96)	39.55	13.85	3413
dsb-2(me96); dsb-1(1A)	93.96	1.40	3370
dsb-2(me96); dsb-1(2A)	83.12	3.31	2413
dsb-2(me96); dsb-1(3A)	97.56	0.64	2395
dsb-2(me96); dsb-1(5A)	98.64	0.04	1596
pph-4.1(tm1598); dsb-1(1A)	7.39	32.21	496
pph-4.1(tm1598); dsb-1(5A)	40.89	7.89	1273

Table 3.1 Embryonic viability and incidence of males of the indicated genotypes. Embryonic viability, male progeny percentage indicating the rate of X chromosome nondisjunction, and total number of scored embryos is shown for hermaphrodite self-progeny of the indicated genotypes (Counting in *pph-4.1(tm1598)*, *dsb-1(5A)* and *pph-4.1(tm1598); dsb-1(5A)* mutants was assisted by Xuan Li).

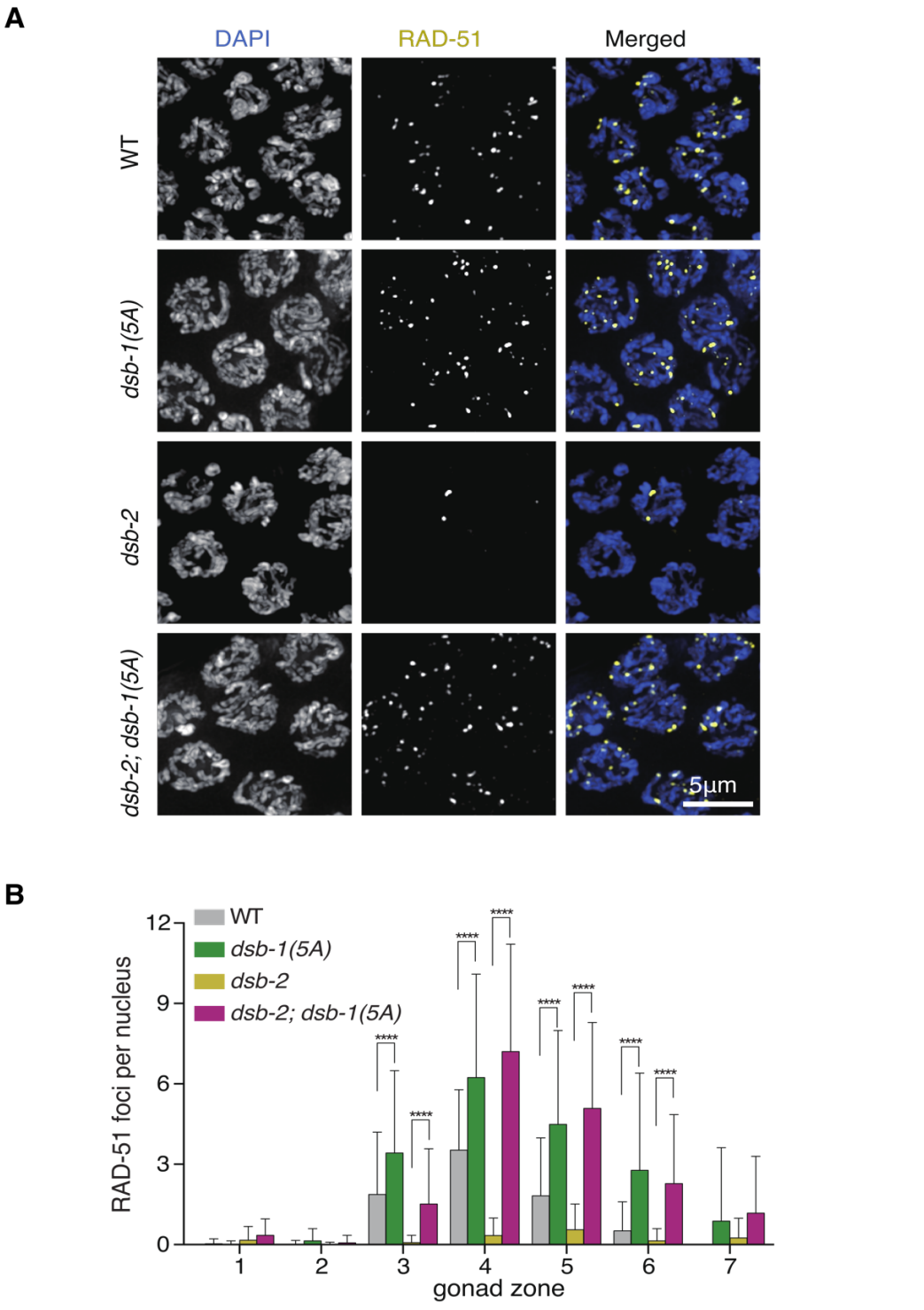

Figure 3.1 The *dsb-1(5A)* mutation rescues DSB formation defects of *dsb-2* mutants. **(A)** Immunofluorescence images of RAD-51 foci in mid-pachytene nuclei of the indicated genotypes. Scale bar, 5 µm. **(B)** Quantification of RAD-51 foci in the gonads of the genotypes indicated in **(A)** (assisted by Minami Murai, Xuan Li and Tjebbe Boersma). Three gonads were scored in *dsb-2(me96)*, *dsb1(5A)* and *dsb-2(me96); dsb-1(5A)* respectively, and two gonads were scored in wild type; the numbers of nuclei scored in zone 1-7 were as follows: for wild type, 57, 99, 112, 123, 109, 62, 27; for *dsb-2(me96)*, 124, 105, 108, 114, 108, 84, 53; for *dsb-1(5A)*, 126, 119, 103, 118, 116, 101, 79; for *dsb-2(me96); dsb-1(5A)*, 94, 131, 118, 91, 93, 96, 71. Significance was assessed via two-tailed *t* test, ****P<0.0001.

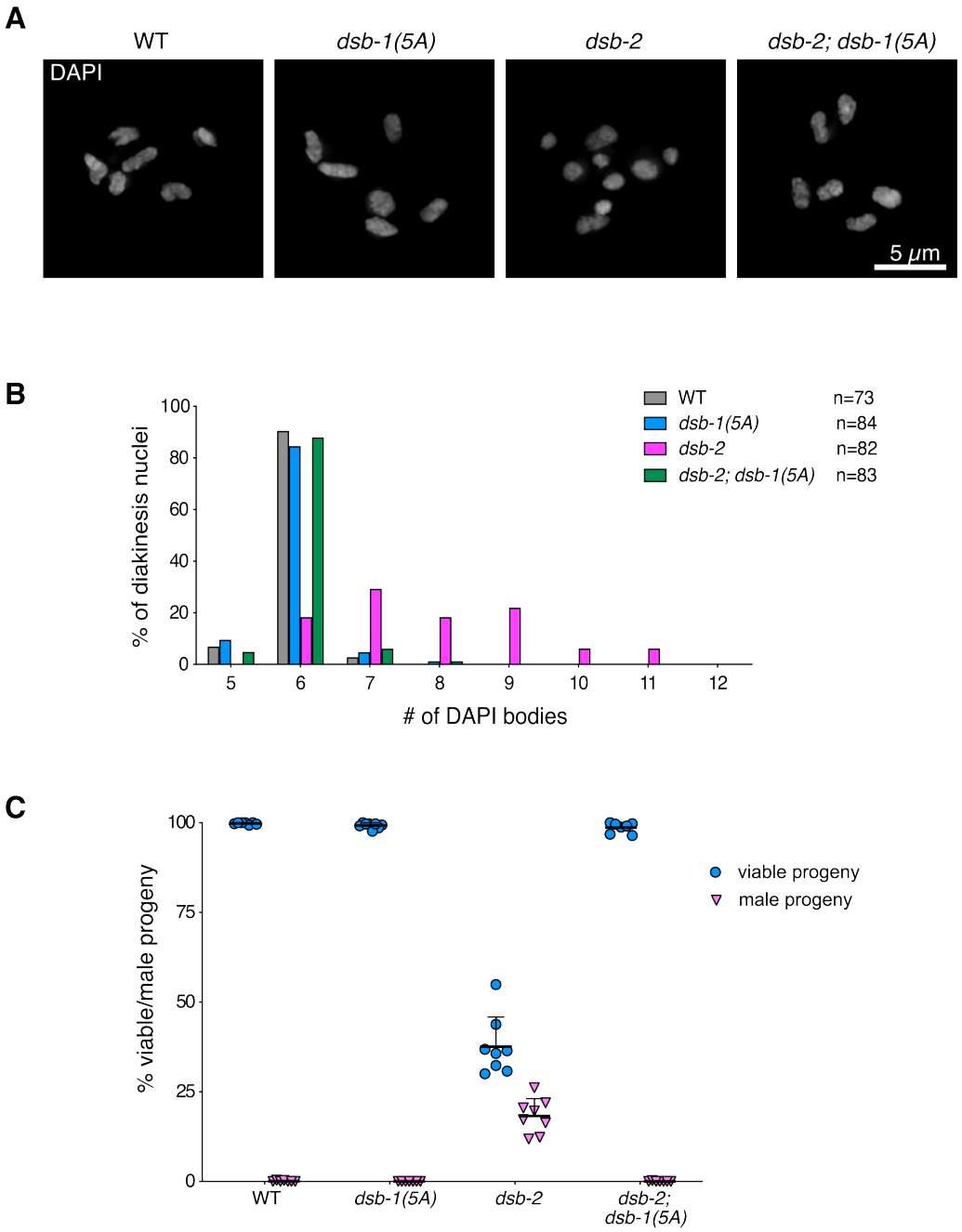

Figure 3.2 The *dsb-1(5A)* mutation rescues CO formation defect of *dsb-2* mutants. (A) Images of DAPI-stained diakinesis nuclei in a wild type animal, a *dsb-1(5A)* mutant, a *dsb-2(me96)* mutant and a *dsb-2(me96); dsb-1(5A)* mutant. Scale bar, 5 µm. **(B)** The number of DAPI-stained bodies shown as percentages of the indicated number of diakinesis oocyte nuclei scored for each genotype. The numbers of nuclei scored for each genotype were: 73 for wild type, 84 for *dsb-1(5A)*, 82 for *dsb-2(me96)*, 83 for *dsb-2(me96); dsb-1(5A)*. **(C)** Embryonic viability percentage and male progeny percentage of wild type animals, *dsb-1(5A)* mutants, *dsb-2(me96)* mutants and *dsb-2(me96); dsb-1(5A)* mutants. Data points are from seven individual animals of wild type, eight individual animals of *dsb-1(5A)*, eight individual animals of *dsb-2(me96)* and seven individual animals of *dsb-2(me96); dsb-1(5A)*.

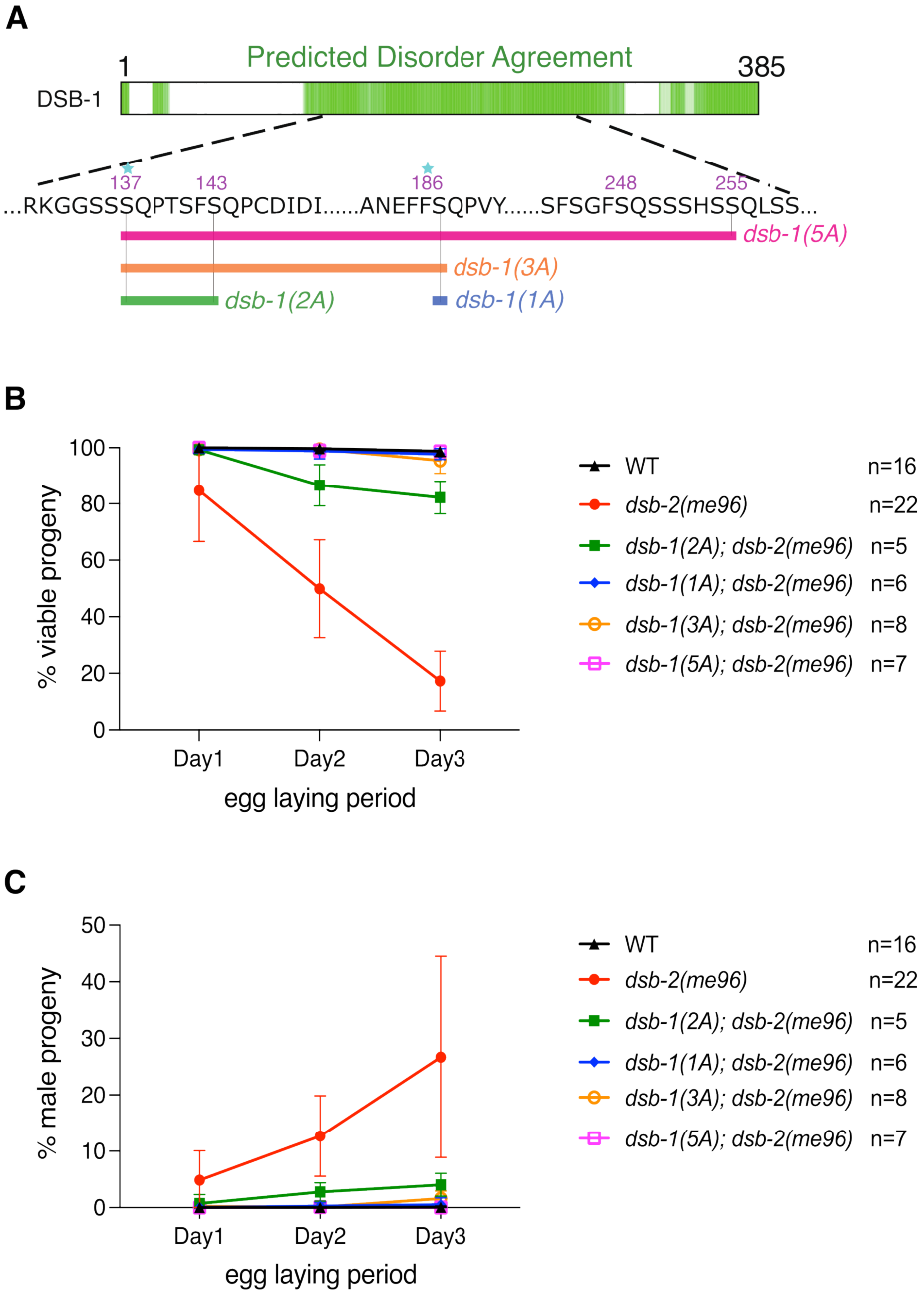

Figure 3.3 Alanine substitution of serine 186 in DSB-1 suffices to rescue the *dsb-2* mutation. **(A)** Diagram depicting a series of *dsb-1* phospho mutants: *dsb-1(1A)* is *dsb-1(S186A)*; *dsb-1(2A)* is *dsb-1(S137A; S143A)*; *dsb-1(3A)* is *dsb-1(S137A; S143A; S186A)* and *dsb-1(5A)* is *dsb-1(S137A; S143A; S186A; S248A; S255A)*. **(B)** The frequency of viable embryos from eggs laid by hermaphrodites of the indicated genotypes during the indicated time interval after the L4 larval stage. **(C)** The frequency of males among surviving progeny from the indicated genotypes during the indicated time interval after the L4 larval stage.

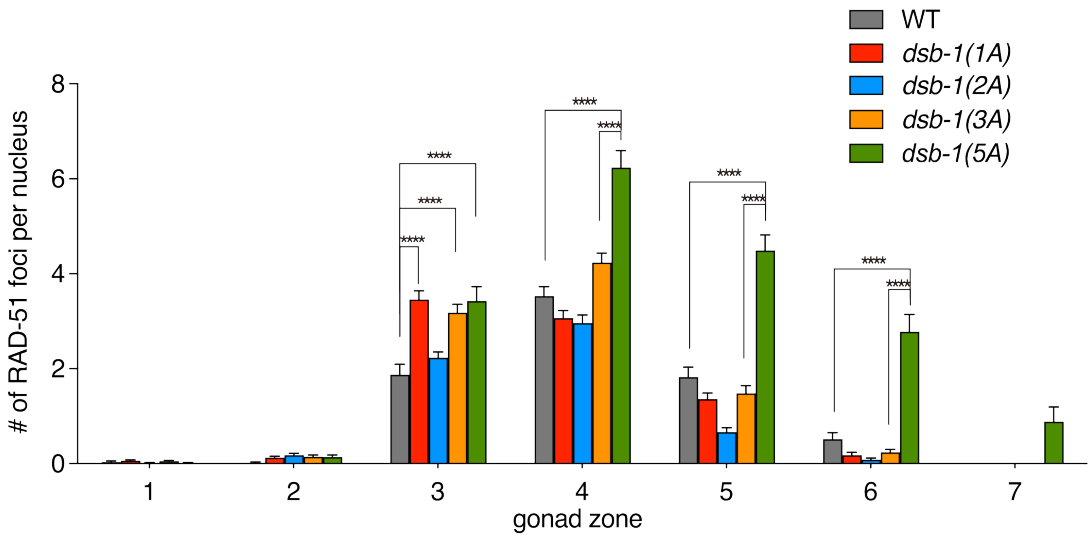

Figure 3.4 DSB formation in a series of *dsb-1* non-phosphorylatable mutants. Quantification of RAD-51 foci in the gonads of the indicated genotypes (data of wild type and *dsb-1(5A)* were duplicated from **Figure 3.1B**). Three gonads were scored for *dsb-1(1A)*, *dsb-1(2A)* and *dsb-1(3A)*; the numbers of nuclei scored in zone 1-7 were as follows: for *dsb-1(1A)*, 147, 183, 191, 169, 133, 84, 22; for *dsb-1(2A)*, 151, 174, 206, 194, 138, 82, 24; for *dsb-1(3A)*, 190, 192, 164, 157, 103, 67, 27. Significance was assessed via two-tailed *t* test, ****P<0.0001.

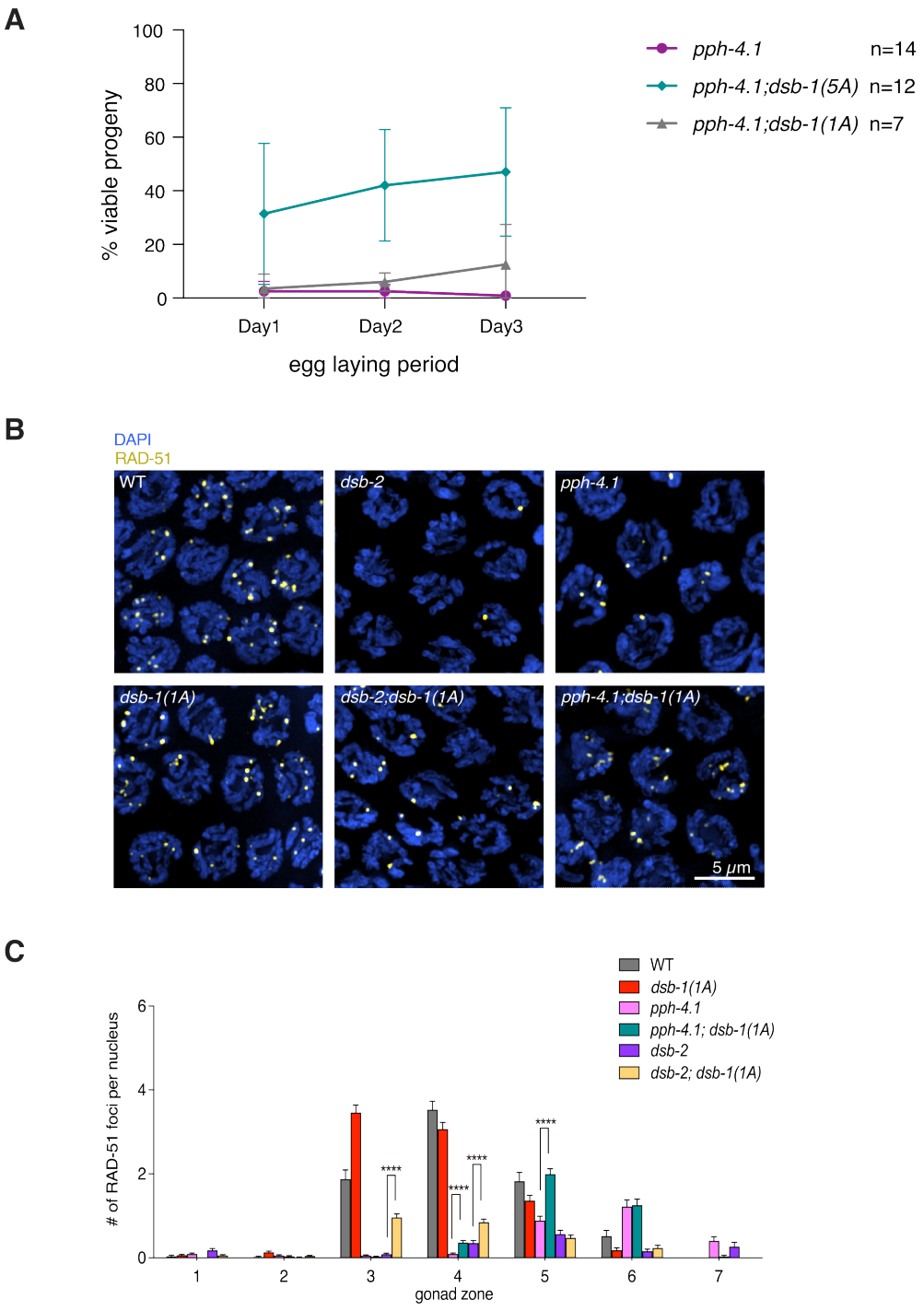

Figure 3.5 The phosphorylation motifs of DSB-1 differentially rescue *dsb-2* and *pph-4.1* mutants. (A) The frequency of viable embryos from eggs laid by hermaphrodites of the indicated genotypes during the indicated time interval after the L4 larval stage. **(B)** Immunofluorescence images of the indicated mutants. Maximum-intensity projections of nuclei at mid-pachytene are shown with DAPI staining in blue and RAD-51 staining in yellow. Scale bar, 5 µm. **(C)** Quantification of RAD-51 foci in the gonads of the genotypes indicated in **(B)** (data of wild type and *dsb-2(me96)* were duplicated from **Figure 3.1B**, data of *pph-4.1(tm1598)* was duplicated from **Figure 2.6B**, data of *dsb-1(1A)* was duplicated from **Figure 3.4**). Three gonads were scored for *dsb-2(me96); dsb-1(1A)* and *pph-4.1(tm1598); dsb-1(1A)*. The numbers of nuclei scored in zone 1-7 were as follows: for *dsb-2(me96); dsb-1(1A)*, 174, 189, 181, 187, 145, 89, 27; for *pph-4.1(tm1598); dsb-1(1A)*, 166, 177, 199, 234, 205, 130, 34. Significance was assessed via two-tailed *t* test, ****P<0.0001.

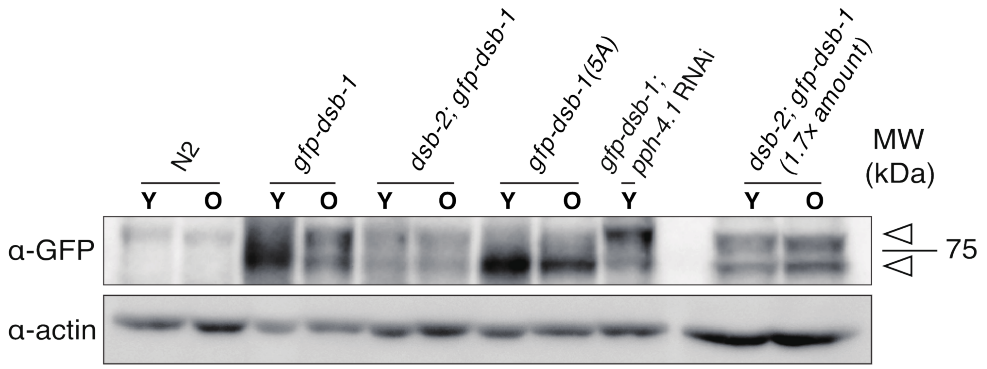

Figure 3.6 Phosphorylation of DSB-1 increases with age in wild type background. Western blots of GFP-fused DSB-1 from young adults (Y, 24 h post-L4 larval stage) and old adults (O, 72h post-L4 larval stage) of the indicated genotypes, probed with α-GFP; arrowheads indicate the two GFP-DSB-1- specific bands in the blot (performed by Aya Sato-Carlton). A total protein amount of 97 µg was loaded in each lane except for the two lanes of *dsb-2; gfp-dsb-1* double mutants on the right, in which 162 µg protein was loaded in each lane. Loading controls (α-actin) are shown at bottom.

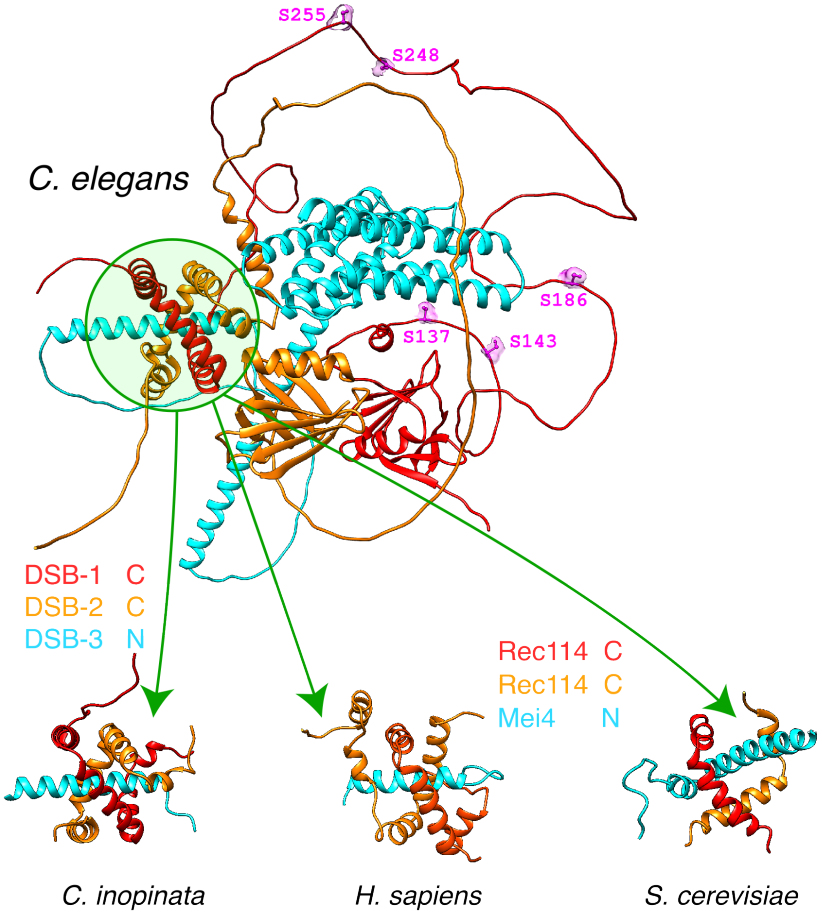

Figure 3.7 Structural prediction of double-strand break factors. A representative structure of the DSB-1, DSB-2, and DSB-3 heterotrimer predicted by the AlphaFold structure prediction pipeline (Jumper et al., 2021; Mirdita, Ovchinnikov, et al., 2021) is shown at top (performed by Peter Carlton). Green circle highlights the region predicted to be the trimerization interface containing the C-termini of DSB-1 and -2, and the N-terminus of DSB-3. ATM/ATR kinase phosphorylation consensus sites in the predicted disordered loop of DSB-1 are shown in magenta and labeled. Sub-regions of similar structures predicted for orthologs of DSB-1, DSB-2, and DSB-3 in the *C. elegans* sister species *Caenorhabditis inopinata*, as well as the putative Rec114/Rec114/Mei4 heterotrimer in human and budding yeast, are shown below. In all cases a predicted N-terminal alpha-helix of the Mei4 ortholog (DSB-3) transfixes a channel formed by the predicted C-terminal helices of the Rec114 orthologs wrapping around each other.

Chapter 4

Discussion and Conclusion

4.1 A model elucidating the control of meiotic DSB formation through DSB-1 phosphoregulation by ATL-1 and PPH-4.1

Studies in other organisms have shown that DSB formation is negatively regulated by ATM/ATR kinases (Carballo et al., 2013; Garcia et al., 2015; Joyce et al., 2011; Lange et al., 2011; Zhang et al., 2011) and it is already known that REC114, a SPO-11 cofactor is phosphorylated by ATM and ATR kinases, which in turn inhibits the DSB formation in budding yeast (Carballo et al., 2013). Moreover, an ortholog of REC114 in *C. elegans* which is DSB-1 has also been investigated and found to be phosphorylated in an ATM/ATR dependent manner, and the phosphorylation also acts to down-regulate DSB formation in order to limit the number of DSBs. In this work, I provide the evidence for the first time that protein phosphatase 4 (PPH-4.1) plays an opposite role, antagonizing ATR kinase rather than ATM kinase to promote DSB formation through the dephosphorylation of DSB-1.

Although it is also possible that PPH-4.1 reduces the phosphorylation of DSB-1 indirectly by dephosphorylating some upstream factors of DSB-1, the basic and the most straightforward model of meiotic DSB formation control in *C. elegans* is that during meiotic prophase, DSB-1 is dephosphorylated by PPH-4.1 to promote a sufficient number of DSBs, which guarantees the successful crossover formation on each paired chromosomes and facilitates the proper chromosome segregation. However, once sufficient recombination intermediates are formed, ATR kinase shuts down the DSB initiation machinery by phosphorylating DSB-1, limiting the DSB numbers and protecting the genome from excessive DNA damage (**Figure 4.1**).

In a word, the balance of meiotic DSB levels is controlled by the phosphoregulation of DSB-1 through ATR kinase and PPH-4.1 phosphatase. The coordinating work of ATR and PPH-4.1 on DSB-1 ensures the success of meiosis progression as well as the integrity of the genome.

4.2 DSBs facilitate the fidelity of homologous pairing and synapsis in *C. elegans*

I have shown that introducing *dsb-1(5A)* mutation into *pph-4.1* background also results in a partial recovery of homologous pairing and synapsis. Although it is known that the initial pairing and synapsis in *C. elegans* does not rely on DSBs since the null mutants of either *spo-11* or *dsb-1* which have a complete loss of DSBs can successfully achieve homologous synapsis (Dernburg et al., 1998; Stamper et al., 2013), I hypothesize that the later stabilization and/or correction of synapsis is dependent on DSBs. It is likely that the hyperphosphorylation of some other substrates in the absence of PPH-4.1 activity results in

promiscuous synapsis in such a low-DSB environment, while providing extra DSBs improve the fidelity of synapsis. Although the exact mechanism of how additional DSBs make the corrections of promiscuous synapsis is still a mystery, one of the possible pathways could be that the increased DSBs enforce the chromosomes to search for their homologs for DNA repair, which in turn provides a higher chance for the chromosomes to find the correct partners. Therefore, the non-homologous synapsis can be corrected through the homologous recombination. However, 50Gy γ-irradiation didn't rescue the failure of CO formation in *pph-4.1* mutants as much as *dsb-1(5A)* allele did, although the γ-ray induced more DSBs than *dsb-1(5A)* allele (data not shown). One explanation is that the exogenous DSBs generated by γ-irradiation are different from the SPO-11-catalyzed DSBs, thus are not capable of correcting the non-homologous synapsis. An alternative explanation is that irradiation triggers not only the double-strand breaks but also the single-strand breaks, which may interfere with the synapsis correction to reach such a level in *pph-4.1; dsb-1(5A)* mutants.

Moreover, *pph-4.1* mutants must need a greater number of DSBs in order to recover their embryonic viability compared to *dsb-2* mutants, since *dsb-1(1A)* allele is sufficient to fully rescue the viability of *dsb-2* mutants but has little effect in *pph-4.1* background. This can be explained by the fact that to restore the embryonic viability of *pph-4.1* mutants, not only the DSB initiation which contributes to the crossover formation but also the promiscuous synapsis needs to be rescued, so more DSBs are needed to solve these problems in a *pph-4.1* background. Given that *pph-4.1; dsb-1(1A)* double mutants have an intermediate number of DSBs between *pph-4.1* and *pph-4.1; dsb-1(5A)* mutants, and furthermore, the non-homologous synapsis due to the absence of PPH-4.1 in *pph-4.1; dsb-1(1A)* mutants is not rescued as well as it is in *pph-4.1; dsb-1(5A)* mutants (**Figure 4.2**), I hypothesize that the number of DSBs required for the corrections of promiscuous synapsis is higher than the one required to guarantee one crossover on each chromosome pair.

In addition, *pph-4.1; dsb-1(5A)* double mutants still exhibit embryonic viability defects, which can be attributed to the incomplete rescue of homologous pairing and synapsis, as well as the incompletely penetrating phenotypes in other processes associated with PPH-4.1, such as centrosome maturation and sperm production (Han et al., 2009; Sumiyoshi et al., 2002) which are not rescued by DSBs.

4.3 DSB-2 plays an auxiliary role in DSB formation

I have shown that the ratio of phosphorylated DSB-1 to unphosphorylated DSB-1 was increased in young adults of *dsb-2* mutants (**Figure 3.6**) and the *dsb-1(1A)* allele is sufficient to fully rescue the loss of embryonic viability in *dsb-2* mutants. These results indicate DSB-2 is involved in antagonizing phosphorylation of DSB-1, which in turn counteracting the anti-DSB activity. As noted in previous studies, loss of *dsb-2* results in a reduction in the amount of DSB-1 protein (Rosu et al., 2013; Stamper et al., 2013), which suggests that DSB-2 may play an auxiliary role in DSB formation by stabilizing DSB-1 protein and compensating for the inactivation of DSB-1, and thus preserve the level of DSBs in old animals.

4.4 *C. elegans* meiocytes have a large capacity to repair excess DSBs over wild type levels

The observation that *dsb-1(5A)* mutants possess a comparable embryonic viability and male progeny frequency to wild type animals in spite of the almost twofold higher number of DSBs suggests that *C. elegans* are tolerant of an increase in DSBs without disrupting the genomic stability. To further test whether *dsb-1(5A)* allele makes the worms more sensitive to exogenous DNA damage or not, both control animals and *dsb-1(5A)* mutants were exposed to either 30 or 70 Gy γ-irradiation. To check the effect of external DSBs on the worms, brood size and embryonic viability of each genotype under the indicated conditions were scored after irradiation. Surprisingly, *dsb-1(5A)* mutants exhibit no difference from control animals in both brood size and embryonic viability (**Figure 4.3**). These results suggest *C.elegans* meiocytes are capable of repairing excess DSBs over wild type levels.

Moreover, it also raises the question of what the negative control of DSBs functions in *C. elegans*. A recent study on the DSB regulation in mice revealed that in the absence of ATM kinase, the dysregulated DSB formation results in more frequent deletions and other rearrangements at the hotspots (Lukaszewicz et al., 2021). Thus, limiting the number of DSBs via the phosphorylation of DSB-1 mediated by ATM kinase in *C. elegans* may prevent such aberrant events from happening and preserve the integrity of the genome over time. Long-term analysis of the genome integrity over generations in *dsb-1(5A)* mutants is a good strategy to address this question in the future.

4.5 Conclusion and future perspectives

In conclusion, this study has shown that the phosphorylation levels of DSB-1 are regulated by ATR kinase and PPH-4.1 phosphatase which work in a counteracting manner. The phosphoregulation of DSB-1 mediates its activity on DSB formation in order to ensure there are not too many but not too few DSBs on each chromosome, which guarantees the formation of crossovers and the correct segregation of chromosomes during meiotic cell division.

However, it is still unknown how the phosphorylation of DSB-1 down-regulates DSB levels. A study on the molecular characterization of *Saccharomyces cerevisiae* RMM (Rec114, Mei4 and Mer2) proteins has shown that neutralizing a conserved basic patch of either REC114 or MER2 disrupts the DNA binding to these proteins (Claeys Bouuaert et al., 2021). Likewise, the negative charge of phosphorylation of DSB-1 may be able to inhibit its interaction with DNA. In addition, the same study discovered that sub-complexes of RMM proteins independently condense with DNA into reversible nucleoprotein clusters that share properties with phase-separated systems (Claeys Bouuaert et al., 2021); which may hint that the phosphorylation of the intrinsically disordered region of DSB-1 could also impact its phase separation properties. *In vivo* studies on DSB-1 and DSB-2 are needed for a better understanding of how much they resemble their yeast orthologs in terms of condensate formation.

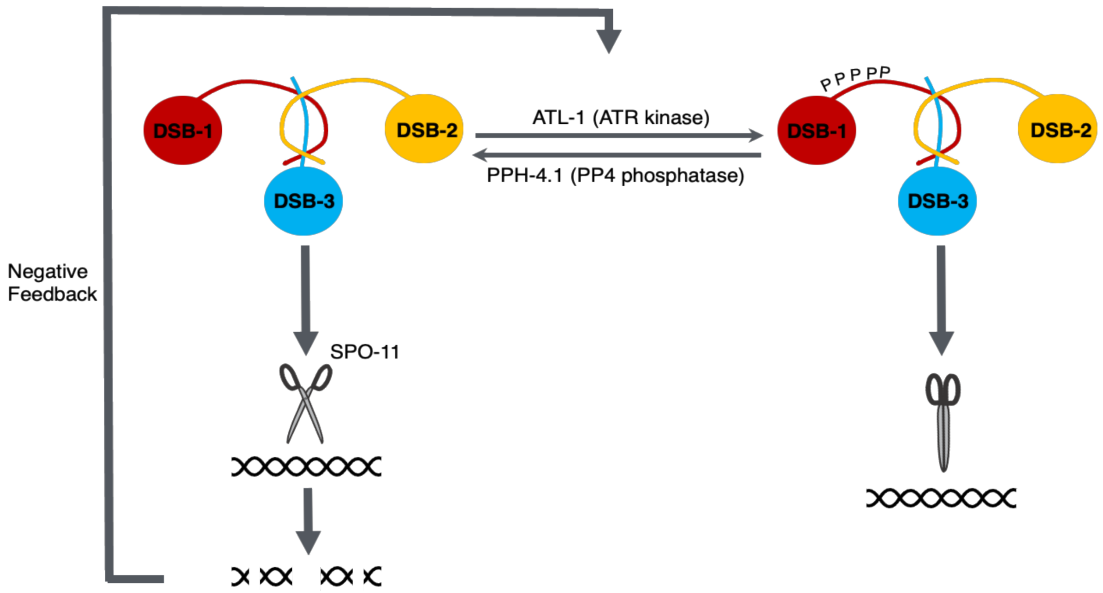

Figure 4.1 A model showing antagonistic action of ATL-1 and PPH-4.1 in DSB-1 regulation. Meiotic DSB levels are regulated through the phosphoregulation of DSB-1 by the opposing activity of ATL-1 (ATR) kinase and PPH-4.1 (PP4) phosphatase, which guarantees a proper number of DSBs for correct chromosome segregation.

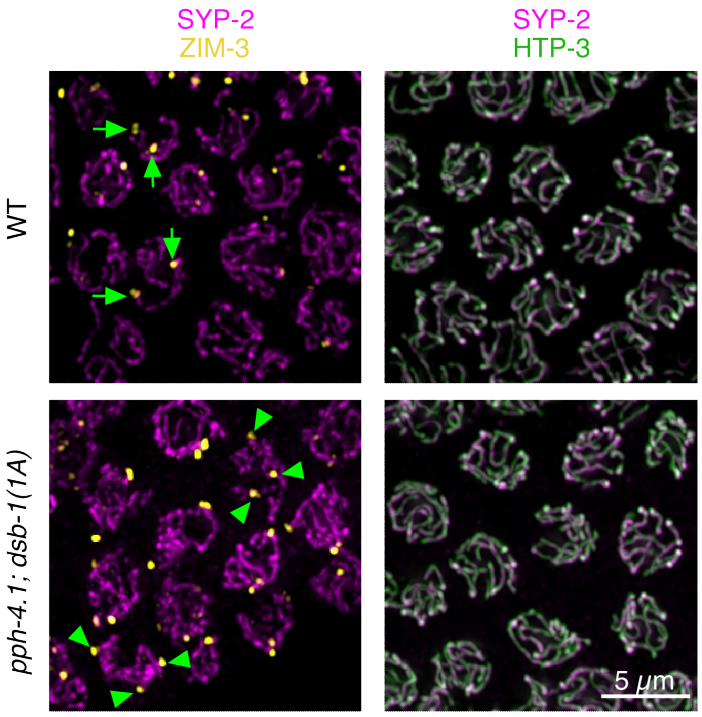

Figure 4.2 Synapsis in *pph-4.1; dsb-1(5A)* mutants. Immunofluorescence images showing the synapsis in wild type and *pph-4.1(tm1598); dsb-1(1A)*. Staining of ZIM-3 (yellow) and SYP-2 (magenta) was used to detect homologous synapsis, arrows in wild type point to examples of two homologously synapsed foci per nucleus, while arrowheads in *pph-4.1(tm1598); dsb-1(1A)* mutant show three synapsed foci, indicating non-homologous synapsis. Full colocalization of HTP-3 (green) and SYP-2 (magenta) in *pph-4.1(tm1598); dsb-1(1A)* mutant as well as wild type indicates the fully synapsed chromosomes. Scale bar, 5 μm.

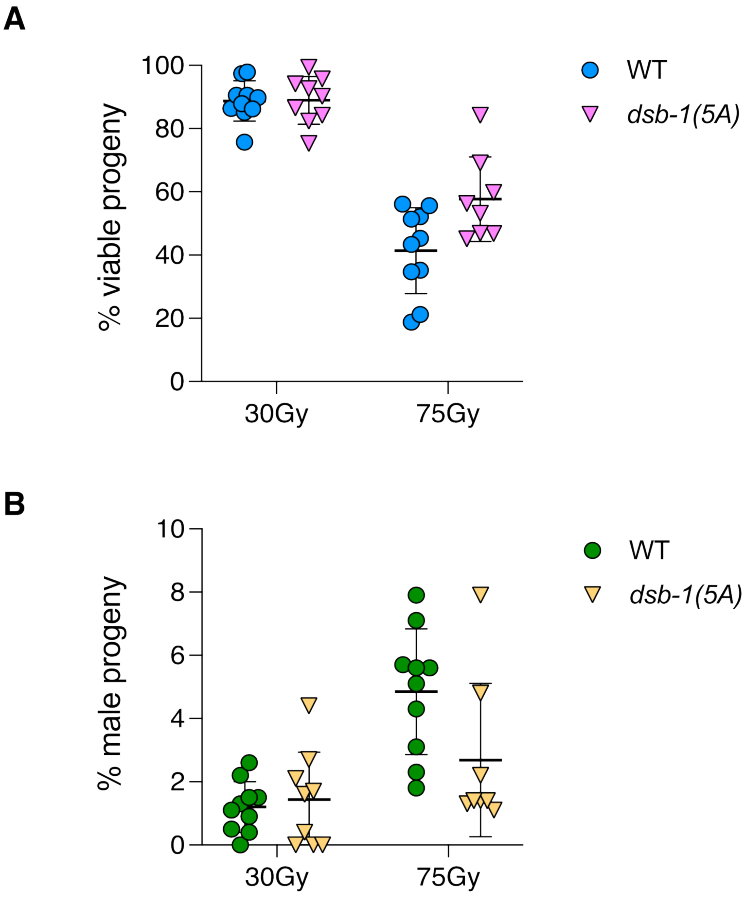

Figure 4.3 The *dsb-1(5A)* mutants do not show sensitivity to exogenous DNA damage. (A) Embryonic viability percentage of wild type and *dsb-1(5A)* mutants exposed to either 30Gy or 75Gy γ-irradiation (assisted by Xuan Li and Masaaki Shimazoe). **(B)** Male progeny percentage of wild type and *dsb-1(5A)* mutants exposed to either 30Gy or 75Gy γ-irradiation**.** Data points in **(A)** and **(B)** are from ten individual animals of wild type (30Gy and 75Gy), nine individual animals of *dsb-1(5A)* (30Gy) and eight individual animals of *dsb-1(5A)* (75Gy).

References

Arribere, J. A., Bell, R. T., Fu, B. X. H., Artiles, K. L., Hartman, P. S., & Fire, A. Z. (2014). Efficient marker-free recovery of custom genetic modifications with CRISPR/Cas9 in Caenorhabditis elegans. *Genetics*, *198*(3), 837–846.

Baudat, F., Manova, K., Yuen, J. P., Jasin, M., & Keeney, S. (2000). Chromosome synapsis defects and sexually dimorphic meiotic progression in mice lacking Spo11. *Molecular Cell*, *6*(5), 989–998.

Bhalla, N., & Dernburg, A. F. (2005). A conserved checkpoint monitors meiotic chromosome synapsis in Caenorhabditis elegans. *Science*, *310*(5754), 1683–1686.

Bishop, D. K., Park, D., Xu, L., & Kleckner, N. (1992). DMC1: a meiosis-specific yeast homolog of E. coli recA required for recombination, synaptonemal complex formation, and cell cycle progression. *Cell*, *69*(3), 439–456.

Blitzblau, H. G., & Hochwagen, A. (2013). ATR/Mec1 prevents lethal meiotic recombination initiation on partially replicated chromosomes in budding yeast. *eLife*, *2*, e00844.

Brenner, S. (1974). The genetics of Caenorhabditis elegans. *Genetics*, *77*(1), 71–94.

Burel, J.-M., Besson, S., Blackburn, C., Carroll, M., Ferguson, R. K., Flynn, H., Gillen, K., Leigh, R., Li, S., Lindner, D., Linkert, M., Moore, W. J., Ramalingam, B., Rozbicki, E., Tarkowska, A., Walczysko, P., Allan, C., Moore, J., & Swedlow, J. R. (2015). Publishing and sharing multi-dimensional image data with OMERO. *Mammalian Genome: Official Journal of the International Mammalian Genome Society*, *26*(9-10), 441–447.

Carballo, J. A., Panizza, S., Serrentino, M. E., Johnson, A. L., Geymonat, M., Borde, V., Klein, F., & Cha, R. S. (2013). Budding yeast ATM/ATR control meiotic double-strand break (DSB) levels by down-regulating Rec114, an essential component of the DSB-machinery. *PLoS Genetics*, *9*(6), e1003545.

Chen, J.-M., Cooper, D. N., Chuzhanova, N., Férec, C., & Patrinos, G. P. (2007). Gene conversion: mechanisms, evolution and human disease. *Nature Reviews. Genetics*, *8*(10), 762–775.

Chin, G. M., & Villeneuve, A. M. (2001). C. elegans mre-11 is required for meiotic recombination and DNA repair but is dispensable for the meiotic G(2) DNA damage checkpoint. *Genes & Development*, *15*(5), 522–534.

Claeys Bouuaert, C., Pu, S., Wang, J., Oger, C., Daccache, D., Xie, W., Patel, D. J., & Keeney, S. (2021). DNA-driven condensation assembles the meiotic DNA break machinery. *Nature*, *592*(7852), 144–149.

Davis, L., & Smith, G. R. (2001). Meiotic recombination and chromosome segregation in Schizosaccharomyces pombe. *Proceedings of the National Academy of Sciences of the United States of America*, *98*(15), 8395–8402.

Dereli, I., Stanzione, M., Olmeda, F., Papanikos, F., Baumann, M., Demir, S., Carofiglio, F., Lange, J., de Massy, B., Baarends, W. M., Turner, J., Rulands, S., & Tóth, A. (2021). Four-pronged negative feedback of DSB machinery in meiotic DNA-break control in mice. *Nucleic Acids Research*. https://doi.org/10.1093/nar/gkab082

Dernburg, A. F., McDonald, K., Moulder, G., Barstead, R., Dresser, M., & Villeneuve, A. M. (1998). Meiotic recombination in C. elegans initiates by a conserved mechanism and is dispensable for homologous chromosome synapsis. *Cell*, *94*(3), 387–398.

Eaton, J. W., Bateman, D., Hauberg, S., & Wehbring, R. (n.d.). *GNU Octave version 5.2. 0 manual: A High-level interactive language for numerical computations, 2019. URL: https*.

Falk, J. E., Chan, A. C.-H., Hoffmann, E., & Hochwagen, A. (2010). A Mec1- and PP4-dependent checkpoint couples centromere pairing to meiotic recombination. *Developmental Cell*, *19*(4), 599–611.

Garcia-Muse, T., & Boulton, S. J. (2005). Distinct modes of ATR activation after replication stress and DNA double-strand breaks in Caenorhabditis elegans. *The EMBO Journal*, *24*(24), 4345–4355.

Garcia, V., Gray, S., Allison, R. M., Cooper, T. J., & Neale, M. J. (2015). Tel1(ATM)-mediated interference suppresses clustered meiotic double-strand-break formation. *Nature*, *520*(7545), 114–118.

Goodyer, W., Kaitna, S., Couteau, F., Ward, J. D., Boulton, S. J., & Zetka, M. (2008). HTP-3 links DSB formation with homolog pairing and crossing over during C. elegans meiosis. *Developmental Cell*, *14*(2), 263–274.

Han, X., Gomes, J.-E., Birmingham, C. L., Pintard, L., Sugimoto, A., & Mains, P. E. (2009). The role of protein phosphatase 4 in regulating microtubule severing in the Caenorhabditis elegans embryo. *Genetics*, *181*(3), 933–943.

Hayashi, M., Chin, G. M., & Villeneuve, A. M. (2007). C. elegans germ cells switch between distinct modes of double-strand break repair during meiotic prophase progression. *PLoS Genetics*, *3*(11), e191.

Hillers, K. J., Jantsch, V., Martinez-Perez, E., & Yanowitz, J. L. (2017). Meiosis. *WormBook: The Online Review of C. Elegans Biology*, *2017*, 1–43.

Hinman, A. W., Yeh, H.-Y., Roelens, B., Yamaya, K., Woglar, A., Bourbon, H.-M. G., Chi, P., & Villeneuve, A. M. (2021a). C. elegans DSB-3 Reveals Conservation and Divergence among Protein Complexes Promoting Meiotic Double-Strand Breaks. In *bioRxiv* (p. 2021.05.14.444243). https://doi.org/10.1101/2021.05.14.444243

Hinman, A. W., Yeh, H.-Y., Roelens, B., Yamaya, K., Woglar, A., Bourbon, H.-M. G., Chi, P., & Villeneuve, A. M. (2021b). Caenorhabditis elegans DSB-3 reveals conservation and divergence among protein complexes promoting meiotic double-strand breaks.

Proceedings of the National Academy of Sciences of the United States of America, *118*(33). https://doi.org/10.1073/pnas.2109306118

Howe, K. L., Bolt, B. J., Shafie, M., Kersey, P., & Berriman, M. (2017). WormBase ParaSite - a comprehensive resource for helminth genomics. *Molecular and Biochemical Parasitology*, *215*, 2–10.

Hunter, N. (2015). Meiotic Recombination: The Essence of Heredity. *Cold Spring Harbor Perspectives in Biology*, *7*(12). https://doi.org/10.1101/cshperspect.a016618

Hunt, P. A., & Hassold, T. J. (2008). Human female meiosis: what makes a good egg go bad? *Trends in Genetics: TIG*, *24*(2), 86–93.

Hustedt, N., Seeber, A., Sack, R., Tsai-Pflugfelder, M., Bhullar, B., Vlaming, H., van Leeuwen, F., Guénolé, A., van Attikum, H., Srivas, R., Ideker, T., Shimada, K., & Gasser, S. M. (2015). Yeast PP4 interacts with ATR homolog Ddc2-Mec1 and regulates checkpoint signaling. *Molecular Cell*, *57*(2), 273–289.

Joyce, E. F., Pedersen, M., Tiong, S., White-Brown, S. K., Paul, A., Campbell, S. D., & McKim, K. S. (2011). Drosophila ATM and ATR have distinct activities in the regulation of meiotic DNA damage and repair. *The Journal of Cell Biology*, *195*(3), 359–367.

Jumper, J., Evans, R., Pritzel, A., Green, T., Figurnov, M., Ronneberger, O., Tunyasuvunakool, K., Bates, R., Žídek, A., Potapenko, A., Bridgland, A., Meyer, C., Kohl, S. A. A., Ballard, A. J., Cowie, A., Romera-Paredes, B., Nikolov, S., Jain, R., Adler, J., … Hassabis, D. (2021). Highly accurate protein structure prediction with AlphaFold. *Nature*, *596*(7873), 583–589.

Kamath, R. S., Fraser, A. G., Dong, Y., Poulin, G., Durbin, R., Gotta, M., Kanapin, A., Le Bot, N., Moreno, S., Sohrmann, M., Welchman, D. P., Zipperlen, P., & Ahringer, J. (2003). Systematic functional analysis of the Caenorhabditis elegans genome using RNAi. *Nature*, *421*(6920), 231–237.

Katoh, K., & Standley, D. M. (2013). MAFFT multiple sequence alignment software version 7: improvements in performance and usability. *Molecular Biology and Evolution*, *30*(4), 772–780.

Keeney, S. (2008). Spo11 and the Formation of DNA Double-Strand Breaks in Meiosis. *Genome Dynamics and Stability*, *2*, 81–123.

Keeney, S., Giroux, C. N., & Kleckner, N. (1997). Meiosis-specific DNA double-strand breaks are catalyzed by Spo11, a member of a widely conserved protein family. *Cell*, *88*(3), 375–384.

Keeney, S., Lange, J., & Mohibullah, N. (2014). Self-organization of meiotic recombination initiation: general principles and molecular pathways. *Annual Review of Genetics*, *48*, 187–214.

Keogh, M.-C., Kim, J., Downey, M., Fillingham, J., Chowdhury, D., Harrison, J. C., Onishi,

M., Datta, N., Galicia, S., Emili, A., & Others. (2006). A phosphatase complex that dephosphorylates γH2AX regulates DNA damage checkpoint recovery. *Nature*, *439*(7075), 497–501.

Kim, J.-A., Hicks, W. M., Li, J., Tay, S. Y., & Haber, J. E. (2011). Protein phosphatases pph3, ptc2, and ptc3 play redundant roles in DNA double-strand break repair by homologous recombination. *Molecular and Cellular Biology*, *31*(3), 507–516.

Kim, S., Peterson, S. E., Jasin, M., & Keeney, S. (2016). Mechanisms of germ line genome instability. *Seminars in Cell & Developmental Biology*, *54*, 177–187.

Kleckner, N. (1996). Meiosis: how could it work? *Proceedings of the National Academy of Sciences of the United States of America*, *93*(16), 8167–8174.

Kumar, R., Ghyselinck, N., Ishiguro, K.-I., Watanabe, Y., Kouznetsova, A., Höög, C., Strong, E., Schimenti, J., Daniel, K., Toth, A., & de Massy, B. (2015). MEI4 – a central player in the regulation of meiotic DNA double-strand break formation in the mouse. *Journal of Cell Science*, *128*(9), 1800–1811.

Kumar, R., Oliver, C., Brun, C., Juarez-Martinez, A. B., Tarabay, Y., Kadlec, J., & de Massy, B. (2018). Mouse REC114 is essential for meiotic DNA double-strand break formation and forms a complex with MEI4. *Life Science Alliance*, *1*(6), e201800259.

Lange, J., Pan, J., Cole, F., Thelen, M. P., Jasin, M., & Keeney, S. (2011). ATM controls meiotic double-strand-break formation. *Nature*, *479*(7372), 237–240.

Lee, D.-H., Pan, Y., Kanner, S., Sung, P., Borowiec, J. A., & Chowdhury, D. (2010). A PP4 phosphatase complex dephosphorylates RPA2 to facilitate DNA repair via homologous recombination. *Nature Structural & Molecular Biology*, *17*(3), 365–372.

Lieber, M. R. (2008). The mechanism of human nonhomologous DNA end joining. *The Journal of Biological Chemistry*, *283*(1), 1–5.

Liu, H., Gordon, S. G., & Rog, O. (2021). Heterologous synapsis in C. elegans is regulated by meiotic double-strand breaks and crossovers. *Chromosoma*, *130*(4), 237–250.

Li, W., & Yanowitz, J. L. (2019). ATM and ATR Influence Meiotic Crossover Formation Through Antagonistic and Overlapping Functions in Caenorhabditis elegans. *Genetics*, *212*(2), 431–443.

Lukaszewicz, A., Lange, J., Keeney, S., & Jasin, M. (2021). De novo deletions and duplications at recombination hotspots in mouse germlines. *Cell*, *184*(24), 5970–5984.e18.

Machovina, T. S., Mainpal, R., Daryabeigi, A., McGovern, O., Paouneskou, D., Labella, S., Zetka, M., Jantsch, V., & Yanowitz, J. L. (2016). A Surveillance System Ensures Crossover Formation in C. elegans. *Current Biology: CB*, *26*(21), 2873–2884.

MacQueen, A. J., & Villeneuve, A. M. (2001). Nuclear reorganization and homologous chromosome pairing during meiotic prophase require C. elegans chk-2. *Genes &*

Development, *15*(13), 1674–1687.

Maleki, S., Neale, M. J., Arora, C., Henderson, K. A., & Keeney, S. (2007). Interactions between Mei4, Rec114, and other proteins required for meiotic DNA double-strand break formation in Saccharomyces cerevisiae. *Chromosoma*, *116*(5), 471–486.

Malone, R. E., Pittman, D. L., & Nau, J. J. (1997). Examination of the intron in the meiosis-specific recombination gene REC114 in Saccharomyces. *Molecular & General Genetics: MGG*, *255*(4), 410–419.

McKim, K. S., Green-Marroquin, B. L., Sekelsky, J. J., Chin, G., Steinberg, C., Khodosh, R., & Hawley, R. S. (1998). Meiotic synapsis in the absence of recombination. *Science*, *279*(5352), 876–878.

McKim, K. S., Howell, A. M., & Rose, A. M. (1988). The effects of translocations on recombination frequency in Caenorhabditis elegans. *Genetics*, *120*(4), 987–1001.

Menees, T. M., & Roeder, G. S. (1989). MEI4, a yeast gene required for meiotic recombination. *Genetics*, *123*(4), 675–682.

Mets, D. G., & Meyer, B. J. (2009). Condensins regulate meiotic DNA break distribution, thus crossover frequency, by controlling chromosome structure. *Cell*, *139*(1), 73–86.

Mirdita, M., Ovchinnikov, S., & Steinegger, M. (2021). ColabFold - Making protein folding accessible to all. In *bioRxiv* (p. 2021.08.15.456425). https://doi.org/10.1101/2021.08.15.456425

Mirdita, M., Schütze, K., Moriwaki, Y., Heo, L., Ovchinnikov, S., & Steinegger, M. (2021). ColabFold - Making protein folding accessible to all. In *Research Square*. https://doi.org/10.21203/rs.3.rs-1032816/v1

Miyazaki, T., Bressan, D. A., Shinohara, M., Haber, J. E., & Shinohara, A. (2004). In vivo assembly and disassembly of Rad51 and Rad52 complexes during double-strand break repair. *The EMBO Journal*, *23*(4), 939–949.

Mohibullah, N., & Keeney, S. (2017). Numerical and spatial patterning of yeast meiotic DNA breaks by Tel1. *Genome Research*, *27*(2), 278–288.

Molnar, M., Parisi, S., Kakihara, Y., Nojima, H., Yamamoto, A., Hiraoka, Y., Bozsik, A., Sipiczki, M., & Kohli, J. (2001). Characterization of rec7, an early meiotic recombination gene in Schizosaccharomyces pombe. *Genetics*, *157*(2), 519–532.

Nadarajan, S., Lambert, T. J., Altendorfer, E., Gao, J., Blower, M. D., Waters, J. C., & Colaiácovo, M. P. (2017). Polo-like kinase-dependent phosphorylation of the synaptonemal complex protein SYP-4 regulates double-strand break formation through a negative feedback loop. *eLife*, *6*. https://doi.org/10.7554/eLife.23437

Oates, M. E., Romero, P., Ishida, T., Ghalwash, M., Mizianty, M. J., Xue, B., Dosztányi, Z., Uversky, V. N., Obradovic, Z., Kurgan, L., Dunker, A. K., & Gough, J. (2012). D2P2: database of disordered protein predictions. *Nucleic Acids Research*, *41*(D1), D508–

D516.

Pattabiraman, D., Roelens, B., Woglar, A., & Villeneuve, A. M. (2017). Meiotic recombination modulates the structure and dynamics of the synaptonemal complex during C. elegans meiosis. *PLoS Genetics*, *13*(3), e1006670.

Phillips, C. M., & Dernburg, A. F. (2006). A family of zinc-finger proteins is required for chromosome-specific pairing and synapsis during meiosis in C. elegans. *Developmental Cell*, *11*(6), 817–829.

Phillips, C. M., McDonald, K. L., & Dernburg, A. F. (2009). Cytological analysis of meiosis in Caenorhabditis elegans. *Methods in Molecular Biology* , *558*, 171–195.

Phillips, C. M., Meng, X., Zhang, L., Chretien, J. H., Urnov, F. D., & Dernburg, A. F. (2009). Identification of chromosome sequence motifs that mediate meiotic pairing and synapsis in C. elegans. *Nature Cell Biology*, *11*(8), 934–942.

Phillips, C. M., Wong, C., Bhalla, N., Carlton, P. M., Weiser, P., Meneely, P. M., & Dernburg, A. F. (2005). HIM-8 binds to the X chromosome pairing center and mediates chromosome-specific meiotic synapsis. *Cell*, *123*(6), 1051–1063.

Raices, M., Bowman, R., Smolikove, S., & Yanowitz, J. L. (2021). Aging Negatively Impacts DNA Repair and Bivalent Formation in the C. elegans Germ Line. *Frontiers in Cell and Developmental Biology*, *9*, 695333.

Roeder, G. S. (1995). Sex and the single cell: meiosis in yeast. *Proceedings of the National Academy of Sciences of the United States of America*, *92*(23), 10450–10456.

Roeder, G. S., & Bailis, J. M. (2000). The pachytene checkpoint. *Trends in Genetics: TIG*, *16*(9), 395–403.

Roelens, B., Schvarzstein, M., & Villeneuve, A. M. (2015). Manipulation of Karyotype in Caenorhabditis elegans Reveals Multiple Inputs Driving Pairwise Chromosome Synapsis During Meiosis. *Genetics*, *201*(4), 1363–1379.

Romanienko, P. J., & Camerini-Otero, R. D. (2000). The mouse Spo11 gene is required for meiotic chromosome synapsis. *Molecular Cell*, *6*(5), 975–987.

Rose, A. M., Baillie, D. L., & Curran, J. (1984). Meiotic pairing behavior of two free duplications of linkage group I in Caenorhabditis elegans. *Molecular & General Genetics: MGG*, *195*(1-2), 52–56.

Rosenbluth, R. E., & Baillie, D. L. (1981). THE GENETIC ANALYSIS OF A RECIPROCAL TRANSLOCATION, *eT1(III; V)*, IN *CAENORHABDITIS ELEGANS*. In *Genetics* (Vol. 99, Issues 3-4, pp. 415–428). https://doi.org/10.1093/genetics/99.3-4.415

Rosu, S., Zawadzki, K. A., Stamper, E. L., Libuda, D. E., Reese, A. L., Dernburg, A. F., & Villeneuve, A. M. (2013). The C. elegans DSB-2 protein reveals a regulatory network that controls competence for meiotic DSB formation and promotes crossover assurance. *PLoS Genetics*, *9*(8), e1003674.

Sato-Carlton, A., Li, X., Crawley, O., Testori, S., Martinez-Perez, E., Sugimoto, A., & Carlton, P. M. (2014). Protein phosphatase 4 promotes chromosome pairing and synapsis, and contributes to maintaining crossover competence with increasing age. *PLoS Genetics*, *10*(10), e1004638.

Sato-Carlton, A., Nakamura-Tabuchi, C., Li, X., Boog, H., Lehmer, M. K., Rosenberg, S. C., Barroso, C., Martinez-Perez, E., Corbett, K. D., & Carlton, P. M. (2020). Phosphoregulation of HORMA domain protein HIM-3 promotes asymmetric synaptonemal complex disassembly in meiotic prophase in Caenorhabditis elegans. *PLoS Genetics*, *16*(11), e1008968.

Shinohara, A., Gasior, S., Ogawa, T., Kleckner, N., & Bishop, D. K. (1997). Saccharomyces cerevisiae recA homologues RAD51 and DMC1 have both distinct and overlapping roles in meiotic recombination. *Genes to Cells: Devoted to Molecular & Cellular Mechanisms*, *2*(10), 615–629.

Shinohara, A., Ogawa, H., & Ogawa, T. (1992). Rad51 protein involved in repair and recombination in S. cerevisiae is a RecA-like protein. *Cell*, *69*(3), 457–470.

Stamper, E. L. (2014). *Meiotic Double-Strand Break Formation in C. elegans* [UC Berkeley]. https://escholarship.org/uc/item/3hn058dz

Stamper, E. L., Rodenbusch, S. E., Rosu, S., Ahringer, J., Villeneuve, A. M., & Dernburg, A. F. (2013). Identification of DSB-1, a protein required for initiation of meiotic recombination in Caenorhabditis elegans, illuminates a crossover assurance checkpoint. *PLoS Genetics*, *9*(8), e1003679.

Stevens, L., Félix, M.-A., Beltran, T., Braendle, C., Caurcel, C., Fausett, S., Fitch, D., Frézal, L., Gosse, C., Kaur, T., Kiontke, K., Newton, M. D., Noble, L. M., Richaud, A., Rockman, M. V., Sudhaus, W., & Blaxter, M. (2019). Comparative genomics of 10 new Caenorhabditis species. *Evolution Letters*, *3*(2), 217–236.

Sumiyoshi, E., Sugimoto, A., & Yamamoto, M. (2002). Protein phosphatase 4 is required for centrosome maturation in mitosis and sperm meiosis in C. elegans. *Journal of Cell Science*, *115*(Pt 7), 1403–1410.

Tessé, S., Bourbon, H.-M., Debuchy, R., Budin, K., Dubois, E., Liangran, Z., Antoine, R., Piolot, T., Kleckner, N., Zickler, D., & Espagne, E. (2017). Asy2/Mer2: an evolutionarily conserved mediator of meiotic recombination, pairing, and global chromosome compaction. *Genes & Development*, *31*(18), 1880–1893.

Traven, A., & Heierhorst, J. (2005). SQ/TQ cluster domains: concentrated ATM/ATR kinase phosphorylation site regions in DNA-damage-response proteins. *BioEssays: News and Reviews in Molecular, Cellular and Developmental Biology*, *27*(4), 397–407.

Villeneuve, A. M. (1994). A cis-acting locus that promotes crossing over between X chromosomes in Caenorhabditis elegans. *Genetics*, *136*(3), 887–902.

Villoria, M. T., Gutiérrez-Escribano, P., Alonso-Rodríguez, E., Ramos, F., Merino, E., Campos, A., Montoya, A., Kramer, H., Aragón, L., & Clemente-Blanco, A. (2019). PP4 phosphatase cooperates in recombinational DNA repair by enhancing double-strand break end resection. *Nucleic Acids Research*, *47*(20), 10706–10727.

Zhang, L., Kim, K. P., Kleckner, N. E., & Storlazzi, A. (2011). Meiotic double-strand breaks occur once per pair of (sister) chromatids and, via Mec1/ATR and Tel1/ATM, once per quartet of chromatids. *Proceedings of the National Academy of Sciences of the United States of America*, *108*(50), 20036–20041.

Zhang, L., Ward, J. D., Cheng, Z., & Dernburg, A. F. (2015). The auxin-inducible degradation (AID) system enables versatile conditional protein depletion in C. elegans. *Development*, *142*(24), 4374–4384.

Zickler, D., & Kleckner, N. (2015). Recombination, Pairing, and Synapsis of Homologs during Meiosis. *Cold Spring Harbor Perspectives in Biology*, *7*(6). https://doi.org/10.1101/cshperspect.a016626